DEVELOPMENTAL BIOLOGY

# Dual and opposing roles for the kinesin-2 motor, KIF17, in Hedgehog-dependent cerebellar development

**Bridget Waas[1], Brandon S. Carpenter[2], Nicole E. Franks[1], Olivia Q. Merchant[1], Kristen J. Verhey[1], Benjamin L. Allen[1]***



**While the kinesin-2 motors KIF3A and KIF3B have essential roles in ciliogenesis and Hedgehog (HH) signal transduction, potential role(s) for another kinesin-2 motor, KIF17, in HH signaling have yet to be explored. Here, we investigated the contribution of KIF17 to HH-dependent cerebellar development, where *Kif17* is expressed in both HH-producing Purkinje cells and HH-responding cerebellar granule neuron progenitors (CGNPs). Germline *Kif17* deletion in mice results in cerebellar hypoplasia due to reduced CGNP proliferation, a consequence of decreased HH pathway activity mediated through decreased Sonic HH (SHH) protein. Notably, Purkinje cell–specific *Kif17* deletion partially phenocopies *Kif17* germline mutants. Unexpectedly, CGNP-specific *Kif17* deletion results in the opposite phenotype—increased CGNP proliferation and HH target gene expression due to altered GLI transcription factor processing. Together, these data identify KIF17 as a key regulator of HH-dependent cerebellar development, with dual and opposing roles in HH-producing Purkinje cells and HH-responding CGNPs.**

## INTRODUCTION

Hedgehog (HH) signaling is a major mitogenic stimulus for postnatal expansion of the developing cerebellum (*1*, *2*). Sonic HH (SHH) ligand is produced by Purkinje cells (PCs) and promotes cerebellar granule neural progenitor (CGNP) proliferation (*1*–*3*). *Shh* deletion within PCs results in cerebellar hypoplasia and reduced CGNP proliferation (*3*). Conversely, increasing the dosage of *Shh* in PCs results in cerebellar hyperplasia and the formation of additional cerebellar lobes (*4*). Genetic deletion of other HH pathway components, namely, *Gli2* (a key transcriptional effector of the HH pathway), *Gas1*, or *Boc* (essential HH pathway coreceptors), within CGNPs leads to cerebellar hypoplasia due to reduced CGNP proliferation (*5*, *6*).

In addition to CGNPs, mature cerebellar granule neurons (CGNs) and BG are HH responsive (*6*). Recent work demonstrated that abrogating HH signaling within BG (through conditional *Smo* deletion) results in a non–cell-autonomous reduction in CGNP proliferation and mild patterning abnormalities (*7*). Notably, the role of HH signaling within mature CGNs remains unclear.

A key organelle that is required for proper HH signaling in mice is the primary cilium [reviewed in (*8*)]. Primary cilia are microtubule-based organelles that project from the cell surface and act as signaling centers for the HH pathway. Anterograde transport within primary cilia is accomplished by the heterodimeric kinesin-2 motor, KIF3A/KIF3B. Loss of either subunit in mice, *Kif3a* or *Kif3b*, leads to an absence of primary cilia, dysregulation of HH signaling, and embryonic lethality (*9*–*11*). Within the developing cerebellum, loss of *Kif3a* within CGNPs leads to cerebellar hypoplasia due to reduced CGNP proliferation and loss of mitogenic response to SHH ligand (*12*). In addition to KIF3A/KIF3B function in ciliogenesis, KIF3A and its adaptor protein, KAP3, regulate HH signaling by binding to and regulating GLI transcription factors (*13*).

The kinesin-2 motor family contains two additional motor complexes in mammals, heterodimeric KIF3A/KIF3C and homodimeric KIF17 [reviewed in (*14*, *15*)]. These motors are known as accessory motors, as they do not have clear roles within mammalian ciliogenesis (*16*–*18*). Loss of *Kif17* is well tolerated across several model organisms, although KIF17 does have defined roles within several neuronal tissues. Within *Caenorhabditis elegans*, loss of OSM-3, a KIF17 homolog, leads to disruption of the distal region of primary cilia in sensory neurons (*19*, *20*). In *Danio rerio*, loss of *Kif17* results in disrupted photoreceptor outer segment development (*21*–*23*) and morphological changes to olfactory cilia (*24*). *Kif17* deletion in mice leads to short-term memory issues, learning disabilities and disruption of NR2B trafficking in the hippocampus (*17*, *25*). Given that KIF17 can alter primary cilia with functional consequences in multiple neuronal cell types across different species, we investigated the contribution of KIF17 to HH signaling during postnatal cerebellar development.

Here, we find that *Kif17* is expressed within SHH-producing PCs and HH-responsive CGNPs. Germline *Kif17* deletion leads to cerebellar hypoplasia, reduced CGNP proliferation, and decreased HH target gene expression across multiple HH-responsive cell types. PC–specific *Kif17* deletion displays similar phenotypes as the germline mutant, demonstrating a requirement for KIF17 in PCs for proper HH signaling, a finding that correlates with reduced SHH protein levels within PCs in *Kif17* mutant animals. Conversely, CGNP-specific *Kif17* deletion results in up-regulation of HH target genes and increased CGNP proliferation in vitro and in vivo, a finding that correlates with reduced GLI3 protein levels (a transcriptional repressor of HH signaling). Together, these data suggest that KIF17 plays dual roles in HH-dependent cerebellar development—promoting HH signaling in PCs through the regulation of SHH ligand and restricting HH signaling in CGNPs through the regulation of GLI transcription factor processing.

## RESULTS

### *Kif17* is expressed within PCs and CGNPs and is required for normal cerebellar development

To investigate a role for the kinesin-2 motor, KIF17, in HH signal transduction, we generated *Kif17* mutant mice on a congenic C5BL/6J background. Specifically, we used $Kif17^{lacZ}$ mice (fig. S1A), where the fourth exon, encoding the motor domain, is replaced with a *lacZ*

[1]Department of Cell and Developmental Biology, University of Michigan, Ann Arbor, MI, 48109, USA. [2]Department of Molecular and Cellular Biology, College of Science and Mathematics, Kennesaw State University, Kennesaw, GA, 30061, USA.
*Corresponding author. Email: benallen@umich.edu

cassette. Similar to previous work on *Kif17* (*17*, *22*), but in contrast to genetic deletion of other kinesin-2 family members (*9*, *10*), *Kif17* homozygous mutant animals are viable and fertile, with no gross morphological abnormalities. Expression analysis revealed that *Kif17* is expressed within the developing cerebellum, starting at postnatal day 4 (P4) and continuing into adulthood (fig. S1, B to G). 5-bromo-4-chloro-3-indolyl-beta-D-galacto-pyranoside (X-GAL) staining of $Kif17^{+/+}$ and $Kif17^{lacZ/lacZ}$ pups at P10 demonstrated *Kif17* expression within the PC layer and, to a lesser degree, within the external granule layer (EGL; Fig. 1, A and B). *Kif17* is expressed in a graded fashion along the anterior-posterior axis, with the strongest signal detected within the posterior lobes (Fig. 1, A and B), not unlike the expression of HH pathway target, *Gli1*, which has increased expression in the posterior lobes compared to the medial lobes at P5 (*6*). To evaluate whether the loss of KIF17 affected the HH-dependent cerebellar development, we continued our analysis of $Kif17^{-/-}$ cerebella at P10, following the peak of HH-dependent CGNP proliferation. For our analysis, we examined mid-sagittal cerebellar sections, where lobes I to III were considered anterior, while lobes VIII to X were considered posterior (fig. S1, H and I).

To identify which cell(s) express *Kif17*, we performed immunofluorescence for β-galactosidase (β-GAL) in $Kif17^{+/+}$ and $Kif17^{lacZ/lacZ}$ cerebella at P10 (Fig. 1, C to H). In posterior lobes of $Kif17^{lacZ/lacZ}$ cerebella, we observed punctate localization of β-GAL within the cell bodies of PCs and in a subset of dendrites (Fig. 1G, arrowheads). Further, we observed β-GAL signal within CGNPs of the EGL (Fig. 1G, bracket). To confirm expression within these two cell populations, we performed fluorescence in situ hybridization in posterior (Fig. 1, I to P) and anterior lobes (fig. S1, J to Q) of $Kif17^{+/+}$ and $Kif17^{lacZ/lacZ}$ cerebella. In both regions of $Kif17^{lacZ/lacZ}$ cerebella, we detected *lacZ* puncta surrounding PC nuclei (Fig. 1, M and N, and fig. S1, N and O) and CGNP nuclei (Fig. 1, O and P, and fig. S1, P and Q), corroborating the β-GAL localization results. Notably, *Kif17* expression was not detected within BGs or mature CGNs. In addition, *Kif17* expression persists in PCs through P21 (fig. S2, A to D). Last, reverse transcription quantitative polymerase chain reaction (RT-qPCR) analysis confirmed *Kif17* expression in CGNPs and verified efficient *Kif17* deletion in mutant animals (fig. S2, E and F). Together, these data indicate that *Kif17* is expressed in two cell populations in the developing cerebellum—SHH-producing PCs and SHH-responsive CGNPs.

While cerebellar area was not significantly reduced in P10 $Kif17^{-/-}$ animals compared to $Kif17^{+/-}$ animals (fig. S2, L to N), analysis of cortical (Fig. 1Q) and cerebellar (Fig. 1R) weights at P10 indicated that *Kif17* mutant cerebella are significantly smaller than $Kif17^{+/+}$ littermates. Notably, this difference persisted even after normalizing cerebellar weight to cortical weight (Fig. 1S). No substantial difference in cortices or cerebellar weights were detected in $Kif17^{+/-}$ animals (fig. S2, G and I). Notably, cerebellar hypoplasia was still observed in *Kif17* mutant animals maintained on a mixed C57BL/6J; 129S4/SvJaeJ background (fig. S2 J). However, this phenotype was not observed in *Kif17* mutants maintained on a congenic 129S4/SvJaeJ background (fig. S2 K). Together, these data suggest that KIF17 promotes cerebellar development, albeit in a genetic background-dependent fashion.

To determine whether KIF17-mediated cerebellar hypoplasia is maintained during cerebellar development, cerebellar weights were measured from P7 to P42 (fig. S2O). While no reduction in cerebellar weight was observed at P7 in $Kif17^{-/-}$ animals, significant reductions were observed at all later time points (fig. S2O). These data suggest that the cerebellar defects observed in *Kif17* mutant animals persist throughout later postnatal cerebellar development and into adulthood.

### *Kif17* germline deletion results in reduced CGNP proliferation and decreased *Gli1* expression within all HH-responsive cells

To assess whether *Kif17* deletion affects CGNPs peak proliferation observed on P7, we examined the percentage of proliferating CGNPs and measured the thickness of the EGL in $Kif17^{+/+}$ and $Kif17^{-/-}$ P7 cerebella (fig. S3, A to L). In both the anterior and posterior regions, we observed reduced EGL thickness but no significant change in the percentage of $Ki67^{+}$/$PAX6^{+}$ CGNPs in the EGL. Considering that *Kif17* expression increases over developmental time and that cerebellar weight is significantly reduced from P10 onward, we evaluated the effects of *Kif17* deletion at P10.

To further investigate which layers of the cerebellum are affected by KIF17 loss, we measured PC dendrite length (Fig. 2A and fig. S4A) and EGL thickness (Fig. 2B and fig. S4B). Although we did not detect significant changes in PC dendrite length, we did observe significant reductions in EGL thickness within both posterior and anterior lobes of $Kif17^{-/-}$ cerebella (Fig. 2B and fig. S4B). Because previous work demonstrated that reduced EGL thickness is associated with a reduction in CGNP proliferation (*5*), we next examined in vivo proliferation of CGNPs in $Kif17^{+/+}$ and $Kif17^{-/-}$ P10 cerebella. Within posterior lobes, we observed a significant reduction in the percentage of $Ki67^{+}$/$PAX6^{+}$ cells and $EdU^{+}$/$PAX6^{+}$ cells in the EGL (Fig. 2, C to J). Within the anterior lobes, we similarly observed a significant reduction in CGNP proliferation (fig. S4, C and D), although to a lesser degree. Intriguingly, while there is a significant reduction in the percentage of $EdU^{+}$ cells, we also observed decreased EdU fluorescence within posterior and anterior lobes of $Kif17^{-/-}$ cerebella (fig. S4, E and F). Together, these data suggest that cerebellar hypoplasia in $Kif17^{-/-}$ mice is due to reduced CGNP proliferation.

To determine whether decreased CGNP proliferation was associated with alterations in the levels of HH signaling in $Kif17^{-/-}$ cerebella, we quantified expression of the HH target gene, *Gli1*, using RT-qPCR and found it is significantly decreased in $Kif17^{-/-}$ P10 cerebella (Fig. 2K). Expression of other HH target genes, *Ptch1*, *Ptch2*, and *Ccnd1*, also trend lower in $Kif17^{-/-}$ cerebella (fig. S4, G to I). Because *Gli1* is expressed in several HH-responsive cells in the developing cerebellum (CGNPs, BGs, and CGNs), section in situ hybridization for *Gli1* was performed to define which cell population(s) displayed down-regulated *Gli1* expression [*Gli1* probe specificity was validated in $Gli1^{-/-}$ cerebella (fig. S4, J to M)]. Unexpectedly, we found that *Gli1* expression is reduced across all HH-responsive cells (Fig. 2, L to Q). In addition, reduced *Gli1* expression persists in CGNs and BG in P21 $Kif17^{-/-}$ cerebella (fig. S4, N to Q). Reduced *Gli1* expression within CGNs could be due to *Kif17* loss in its progenitors, CGNPs. However, because we did not observe *Kif17* expression within BG, we hypothesized that KIF17 acts in a non–cell-autonomous fashion in SHH-producing PCs to regulate *Gli1* expression.

### PC–specific *Kif17* deletion results in a non–cell-autonomous HH loss-of-function phenotype

To directly assess KIF17 function in PCs, we conditionally deleted *Kif17* within PCs using a $Shh^{Cre}$ driver (Fig. 3A). The specificity of $Shh^{Cre}$ was confirmed through breeding with $Rosa26^{LSL\text{-}tdT}$ reporter mice (fig. S5, A to F). Consistent with previous reports (*26*), $Shh^{Cre}$ efficiently mediates recombination in Calbindin (CALB1)–positive

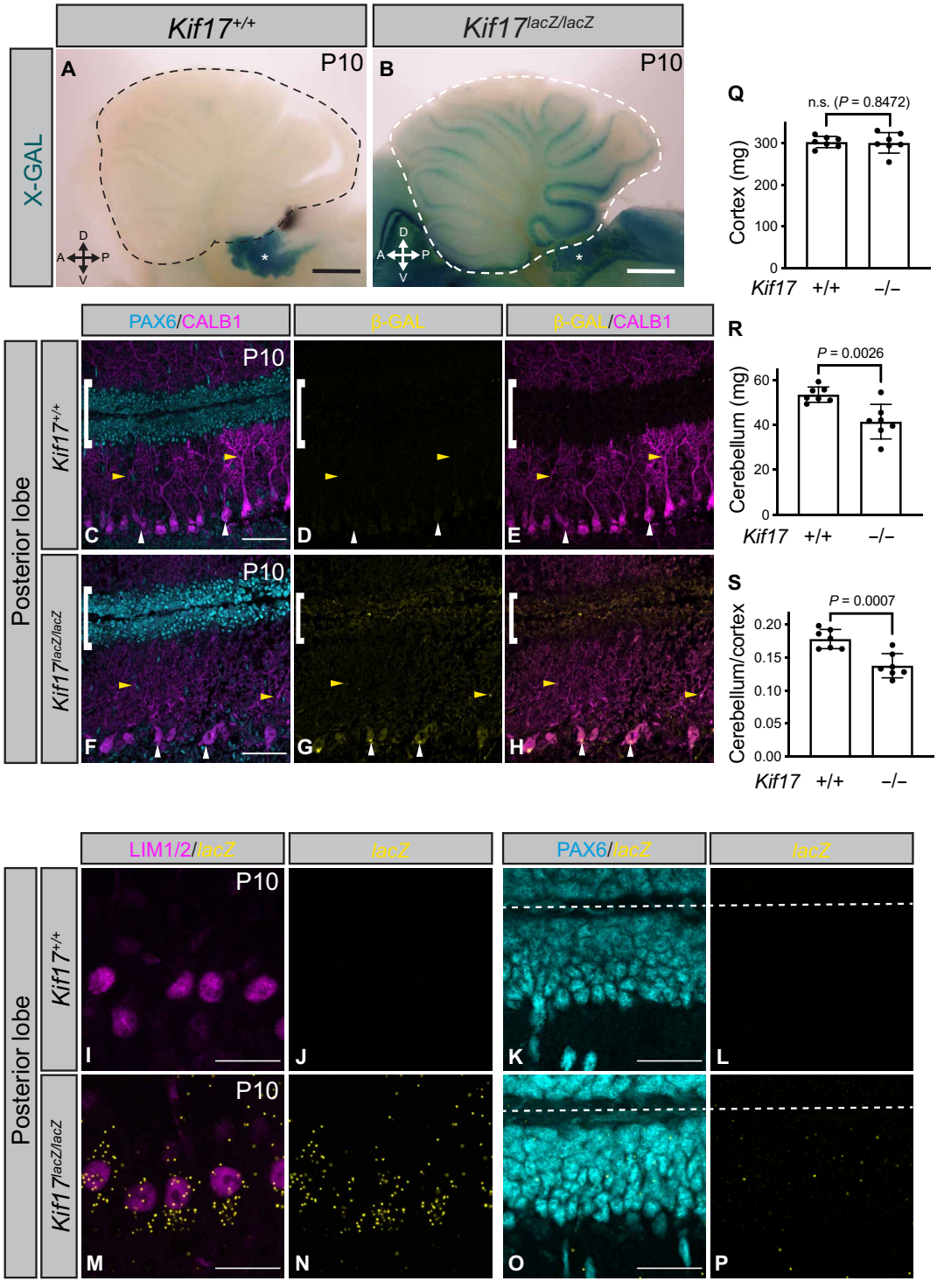


**Fig. 1. *Kif17* is expressed within PCs and CGNPs and is required for normal cerebellar development.** Whole-mount X-GAL staining of *Kif17*$^{+/+}$ (**A**) and *Kif17*$^{lacZ/lacZ}$ (**B**) cerebella at P10. Scale bars, 500 μm. Asterisks denote endogenous β-GAL activity in the choroid plexus (*70*). Immunofluorescent antibody detection of β-GAL (yellow) in *Kif17*$^{+/+}$ (**C** to **E**) and *Kif17*$^{lacZ/lacZ}$ (**F** to **H**) P10 posterior cerebellar lobes. Antibody detection of PAX6 (cyan) and Calbindin (CALB1, magenta) mark granule neuron nuclei and PCs, respectively. White brackets denote the EGLs, white arrowheads indicate PC cell bodies, and yellow arrowheads indicate PC dendrites. Scale bars, 50 μm [(C) and (F)]. Fluorescent in situ detection of *lacZ* mRNA (yellow; I to P) in *Kif17*$^{+/+}$ (**I** to **L**) and *Kif17*$^{lacZ/lacZ}$ (**M** to **P**) P10 cerebella. Antibody detection of LIM1/2 [magenta; (I) and (M)] and PAX6 [cyan; (K) and (O)] identify PC and CGNP nuclei, respectively. Dashed lines separate individual EGLs. Scale bars, 25 μm [(I), (K), (M), and (O)]. Quantitation of cortex weight (**Q**), cerebellar weight (**R**), and cerebellar weight normalized to cortex weight (**S**) in P10 *Kif17*$^{+/+}$ and *Kif17*$^{-/-}$ mice. Data are mean ± SD. Each dot represents an individual animal. *P* values were determined by a two-tailed Student's *t* test. n.s., not significant.

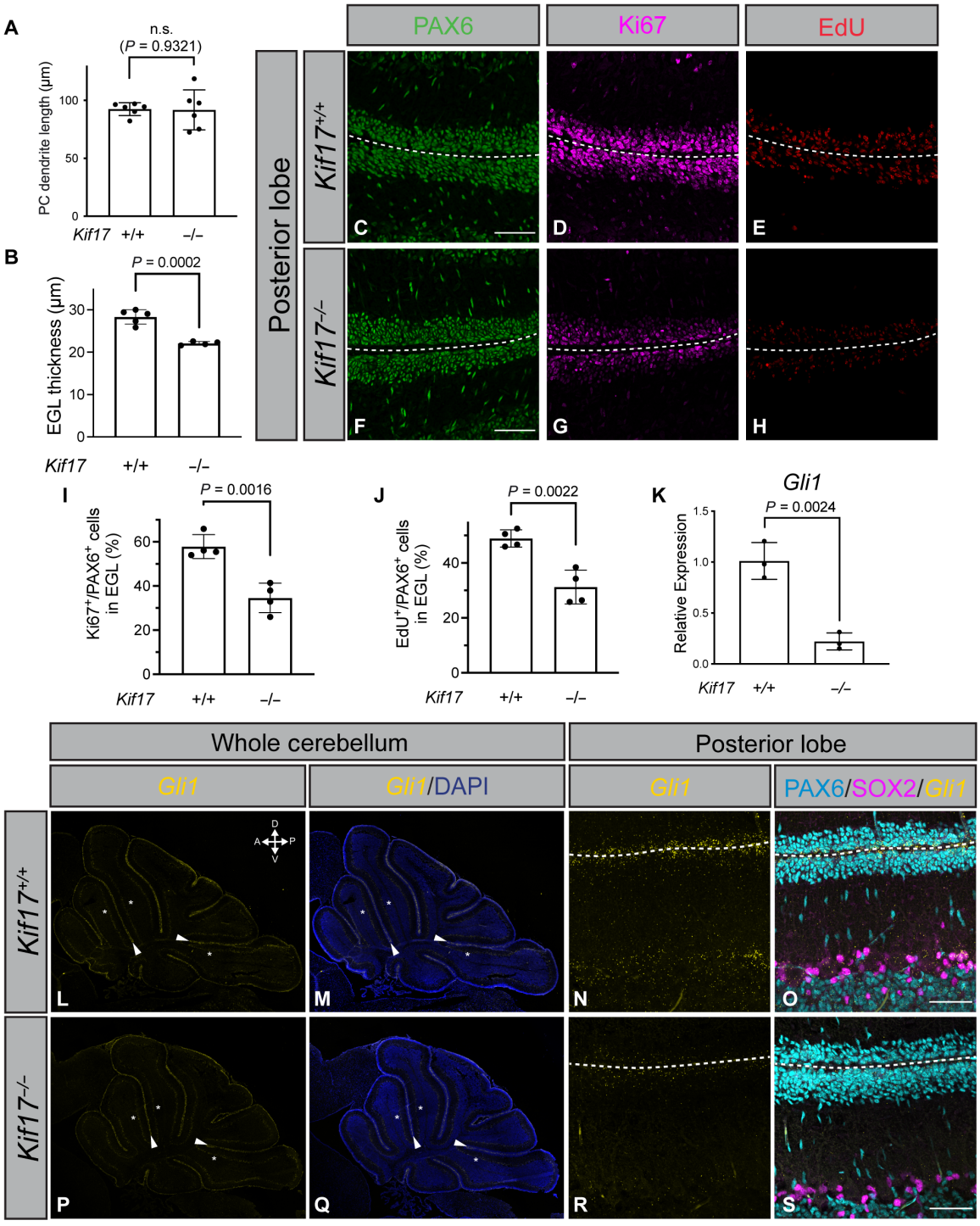


**Fig. 2. *Kif17* germline deletion results in reduced CGNP proliferation and decreased *Gli1* expression within all HH-responsive cells.** Quantitation of PC dendrite length (**A**) and EGL (**B**) thickness in posterior lobes of P10 *Kif17*$^{+/+}$ and *Kif17*$^{-/-}$ cerebella. Immunofluorescent analysis of CGNP proliferation in the posterior lobes of P10 *Kif17*$^{+/+}$ (**C** to **E**) and *Kif17*$^{-/-}$ (**F** to **H**) cerebella. Antibody detection of PAX6 [green; (C) and (F)] and Ki67 [magenta; (D) and (G)]. Fluorescent azide detection of EdU [red; (E) and (H)]. Scale bars, 50 µm [(C) and (F)]. Dashed line separates individual EGLs. Percentage of Ki67$^{+}$/PAX6$^{+}$ (**I**) and EdU$^{+}$/PAX6$^{+}$ (**J**) cells within the posterior lobes of P10 *Kif17*$^{+/+}$ and *Kif17*$^{-/-}$ cerebella. RT-qPCR detection of *Gli1* expression (**K**) in P10 *Kif17*$^{+/+}$ and *Kif17*$^{-/-}$ cerebella. Data are mean ± SD. Each dot represents the average of three to five images per individual animal [(A) and (B) and (I) and (J)] or an individual animal (K). *P* values were determined by a two-tailed Student's *t* test. (**L** to **S**) Fluorescent in situ hybridization detection of *Gli1* (yellow) in *Kif17*$^{+/+}$ [(L) to (O)] and *Kif17*$^{-/-}$ [(P) to (S)] P10 cerebella. Whole cerebellar sections [(L), (M), (P), and (Q)] counterstained with 4′,6-diamidino-2-phenylindole (DAPI) (blue). Arrowheads [(L), (M), (P), and (Q)] point to the EGL (CGNPs), while asterisks denote the IGL, containing CGNs. Posterior lobe images [(N), (O), (R), and (S)] with antibody detection [(O) and (S)] of PAX6 (cyan) and SOX2 (magenta) to label CGNs and BG, respectively. Scale bars, 500 µm [(L) and (O)] and 50 µm [(N) and (Q)]. Dashed lines separate EGLs.

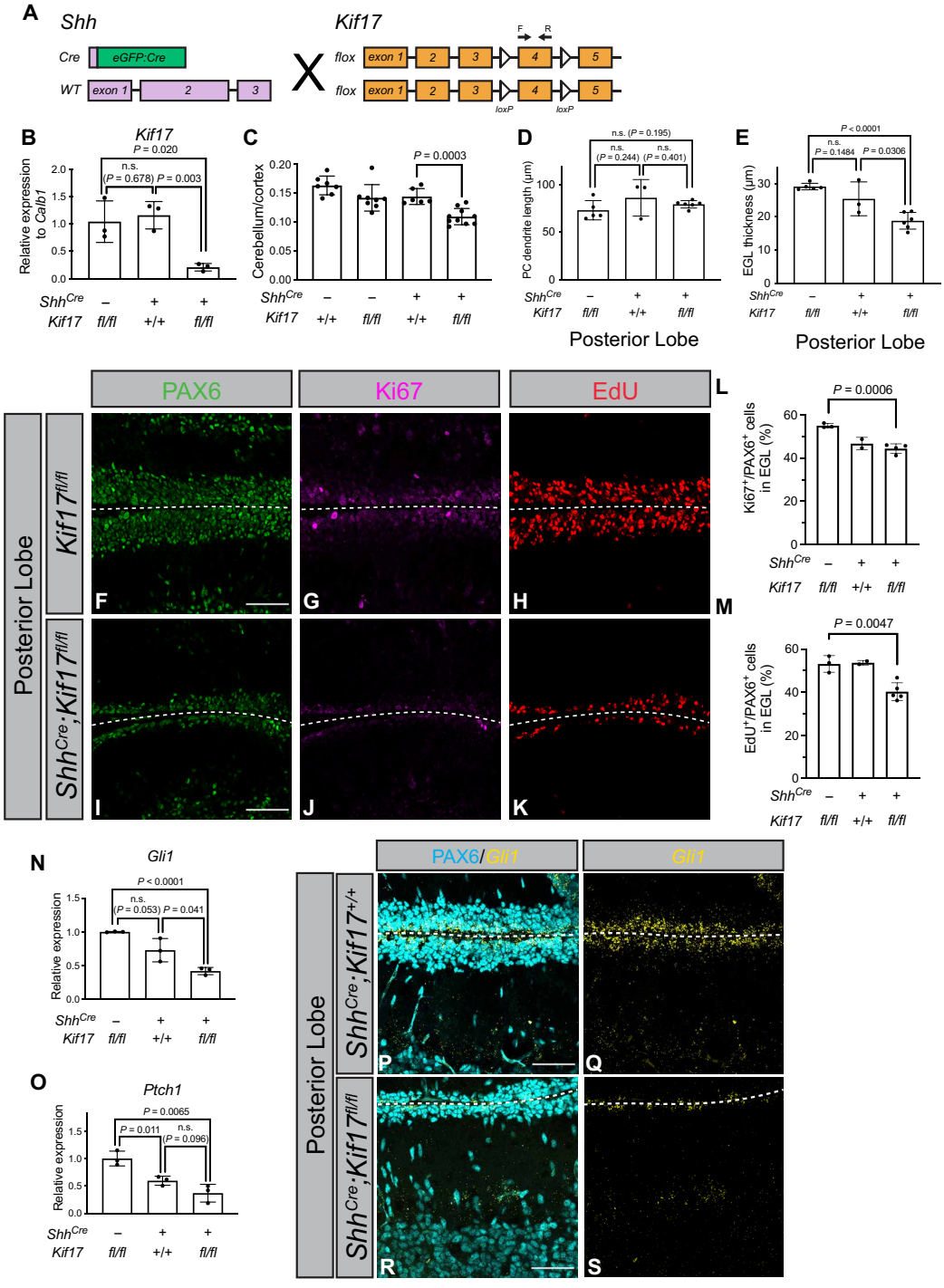


**Fig. 3. PC–specific *Kif17* deletion results in a non–cell-autonomous HH loss-of-function phenotype.** (**A**) Schematic representing conditional *Kif17* deletion within PCs using $Shh^{Cre}$. Arrows above exon 4 denote qPCR primers. Relative *Kif17* expression (**B**) by RT-qPCR in $Kif17^{fl/fl}$, $Shh^{Cre}$;$Kif17^{+/+}$, and $Shh^{Cre}$;$Kif17^{fl/fl}$ P10 whole cerebella. Cerebellum weight normalized to cortex weight (**C**) P10 in P10 control and PC–specific *Kif17* deletion mice. Quantitation of PC dendrite length (**D**) and EGL (**E**) thickness within posterior lobes of P10 cerebella in $Kif17^{fl/fl}$, $Shh^{Cre}$;$Kif17^{+/+}$, and $Shh^{Cre}$;$Kif17^{fl/fl}$ mice. Immunofluorescent analysis of CGNP proliferation in $Kif17^{fl/fl}$ (**F** to **H**) and $Shh^{Cre}$;$Kif17^{fl/fl}$ (**I** to **K**) P10 cerebella. Antibody detection of PAX6 [green; (F) and (I)] and Ki67 [magenta; (G) and (J)]. Fluorescent azide detection of EdU [red; (H) and (K)]. Scale bars, 50 µm [(F) and (I)]. Percentage of $Ki67^{+}$/$PAX6^{+}$ (**L**) and $EdU^{+}$/$PAX6^{+}$ (**M**) cells within the posterior lobes in P10 control and conditional *Kif17* deletion cerebella. Relative expression of *Gli1* (**N**) and *Ptch1* (**O**) measured by RT-qPCR in P10 whole cerebella in $Kif17^{fl/fl}$, $Shh^{Cre}$;$Kif17^{+/+}$, and $Shh^{Cre}$;$Kif17^{fl/fl}$ mice. Data are mean ± SD. Each dot represents an individual animal [(B) and (C) and (N) and (O)] or an average of five images per animal [(D) and (E) and (L) and (M)]. *P* values were determined by a two-tailed Student's *t* test. Fluorescent in situ detection of *Gli1* (yellow; **P** to **S**) and antibody detection of PAX6 [cyan; (P) and (R)] within posterior cerebellar lobes of P10 $Shh^{Cre}$;$Kif17^{+/+}$ [(P) and (Q)] and $Shh^{Cre}$;$Kif17^{fl/fl}$ [(R) and (S)] mice. Scale bars, 50 µm [(P) and (R)]. Dashed lines separate EGLs.

PCs. $Shh^{Cre}$ is a loss-of-function allele; however, reducing *Shh* dosage does not alter cerebellar size in $Kif17^{-/-};Shh^{+/-}$ pups compared to $Kif17^{-/-}$ littermates (fig. S5G). RT-qPCR analysis revealed significantly reduced *Kif17* expression in $Shh^{Cre};Kif17^{fl/fl}$ cerebella (Fig. 3B), suggesting efficient deletion within PCs (note that residual *Kif17* expression is likely due to the presence of *Kif17*-expressing CGNPs). PC–specific *Kif17* deletion results in cerebellar hypoplasia measured by cerebellar weight (Fig. 3C and fig. S5H) and cerebellar area (fig. S5, I to K), reminiscent of *Kif17* germline deletion (cf. Fig. 1S and fig. S2, L to N).

As with *Kif17* germline mutants, PC dendrite length is unaltered in PC–specific *Kif17* mutant pups in either posterior (Fig. 3D) or anterior (fig. S5L) lobes. However, there is a significant reduction in EGL thickness, specifically in posterior lobes (Fig. 3E and fig. S5M). Consistent with $Kif17^{-/-}$ mice, analysis of CGNP proliferation revealed a significant reduction in the percentage $Ki67^{+}$ cells and $EdU^{+}$ cells within both the posterior and anterior lobes of $Shh^{Cre:GFP};Kif17^{fl/fl}$ mice compared to control littermates (Fig. 3, F to M, and fig. S5, N and O). In addition, we observed significant reductions in the expression of multiple HH target genes, including *Gli1* and *Ptch1* (Fig. 3, N and O) as well as *Ptch2* and *Ccnd1*, as measured by RT-qPCR (fig. S5, P and Q). Fluorescence in situ hybridization revealed reduced *Gli1* expression in $Shh^{Cre:GFP};Kif17^{fl/fl}$ cerebella within CGNPs, BGs, and CGNs (Fig. 3, P to S). These data demonstrate that PC–specific *Kif17* deletion partially phenocopies germline *Kif17* mutant cerebella through reduced EGL thickness, decreased CGNP proliferation, and down-regulation of HH target genes. One possibility is that the HH loss-of-function phenotype could be due to PC alterations. While we did observe an overall reduction in the number of PCs per section with *Kif17* deletion (fig. S5, R to U), we did not observe any gross differences in PC morphology or density in either *Kif17* germline deletion or PC-specific *Kif17* deletion cerebella (fig. S5, V to AA).

Moreover, defective ciliogenesis is associated with the loss of PCs (*27*), and deletion of *OSM-3/Kif17* results in primary cilia defects in *C. elegans* and *D. rerio* (*19*–*24*). However, we did not observe a significant difference in PC ciliary length within the anterior and posterior lobes of P10 $Kif17^{+/+}$ and $Kif17^{-/-}$ cerebella (fig. S6, A to F). Together, these data establish an essential role for KIF17 within SHH-producing PCs during cerebellar development.

## KIF17 regulates SHH protein in the developing posterior cerebellum

The reduction of HH target gene expression across multiple HH-responsive cells in *Kif17* mutant cerebella suggested a non–cell-autonomous role for KIF17 in HH signal transduction. Given that SHH, the only HH ligand expressed in the developing cerebellum, is produced by PCs, we explored a role for KIF17 in PC regulation of SHH localization and release. Initially, examination of *Shh* expression by RT-qPCR revealed that *Shh* transcripts are down-regulated in both $Kif17^{-/-}$ mice (Fig. 4A) and PC–specific conditional *Kif17* mutants (Fig. 4B). Next, we assessed the protein levels of SHH ligand and observed that levels of N-terminal SHH (N-SHH) are subtly, but not significantly, decreased in the cerebella of *Kif17* germline mutants [Fig. 4, C and D; SHH antibody specificity was validated in $Shh^{-/-}$ tissue (fig. S6G)].

We also examined levels of the HH coreceptor, BOC, which is expressed in PCs (*5*) and has been recently demonstrated to regulate SHH localization in cytonemes of NIH/3T3 cells (*28*). Notably, levels of *Boc* transcripts (fig. S6, H and I) and BOC protein are unaltered in *Kif17* mutant cerebella (fig. S6, J and K). However, *Scube2*, which encodes a key regulator of SHH protein release (*29*, *30*), is significantly reduced in P10 cerebella from both $Kif17^{-/-}$ (Fig. 4E) and PC–specific *Kif17* mutant animals (Fig. 4F). Given the reduced levels of *Scube2*, we speculated that KIF17 could affect SHH ligand release or secretion.

To assess a role for KIF17 in SHH release, we used a gain-of-function approach, where COS-7 cells were driven to express epitope-tagged KIF17 [KIF17:hemagglutinin (HA)] and either full length [SHH:green fluorescent protein (GFP)] or N-SHH (Fig. 4G). While KIF17 expression does not alter the levels of secreted N-SHH (fig. S6L), we did observe increased levels of secreted full-length SHH (Figure 4H). We also observed significantly increased levels of intracellular SHH, including full-length SHH:GFP, N-SHH:GFP, and N-SHH when co-expressed with KIF17 (Fig. 4I and fig. S6, M and N).

To investigate KIF17-mediated regulation of intracellular SHH levels in vivo, we used an antibody directed toward the C terminus of SHH [SHH antibody specificity was validated in P10 cerebella of *Shh* conditional mutant animals ($Shh^{CreER/lacZ}$; fig. S6, O to W)]. Intracellular SHH is detected in the Golgi/endoplasmic reticulum (horizontal arrowheads) and within the cell bodies of PCs of $Kif17^{+/-}$ and $Kif17^{-/-}$ littermates (vertical arrowheads, Fig. 4, J to M, and fig. S6, X and Y). However, SHH levels are significantly reduced in the posterior lobes of $Kif17^{-/-}$ P10 cerebella (Fig. 4N). Notably, SHH levels are not significantly altered in anterior lobes of $Kif17^{-/-}$ mice (fig. S6Z). Given that intracellular SHH is not significantly altered in anterior lobes, these data provide an explanation for the lack of a statistically significant reduction in SHH protein in whole cerebellar lysates (Fig. 4, C and D). Together, these gain- and loss-of-function data suggest that KIF17 acts in PCs to stabilize intracellular SHH protein and promote SHH release specifically within the posterior lobes. This is supported by the down-regulation of HH target genes across the multiple HH-responsive cell types (CGNPs, BGs, and CGNs) following PC–specific *Kif17* deletion. We propose that the reduction of SHH protein ultimately results in decreased CGNP proliferation and cerebellar hypoplasia in *Kif17* deletion mice (Fig. 4O).

## *Kif17* deletion promotes CGNP proliferation in vitro

To investigate a role for KIF17 in CGNPs, we isolated and cultured wild-type and $Kif17^{-/-}$ CGNPs in vitro (*31*). HH-dependent proliferation was measured in response to treatment with either smoothened agonist (SAG) or N-SHH conditioned media (N-SHH CM). Unexpectedly, $Kif17^{-/-}$ CGNPs display increased baseline proliferation compared to $Kif17^{+/-}$ and $Kif17^{+/+}$ CGNPs (fig. S7, A to G). Treatment with either SAG or N-SHH CM resulted in increased CGNP proliferation, as measured by EdU/5-bromo-2′-deoxyuridine (BrdU) incorporation (fig. S7, E and F) or luminescence-based quantitation of adenosine 5′-triphosphate levels (fig. S7G). In addition, we cultured CGNPs from $Kif17^{fl/fl}$ and $Shh^{Cre};Kif17^{fl/fl}$ littermates and evaluated their proliferation in vitro (fig. S7, H to M). We observed no significant differences of CGNP proliferation in $Kif17^{fl/fl}$ and $Shh^{Cre};Kif17^{fl/fl}$ cultures, confirming increased proliferation in $Kif17^{-/-}$ CGNPs is a cell-autonomous phenotype. Notably, these results are distinct from those observed in CGNPs lacking *Boc*, which encodes for an essential HH coreceptor (*5*). Direct comparison of $Kif17^{-/-}$ CGNP and $Boc^{-/-}$ CGNP proliferation confirmed that *Kif17* deletion results in increased baseline and HH-stimulated CGNP proliferation (fig. S8A). These data contrast with CGNP proliferation in vivo (cf. Fig. 2, C to J), suggesting distinct and opposing roles for KIF17 in PCs and CGNPs.

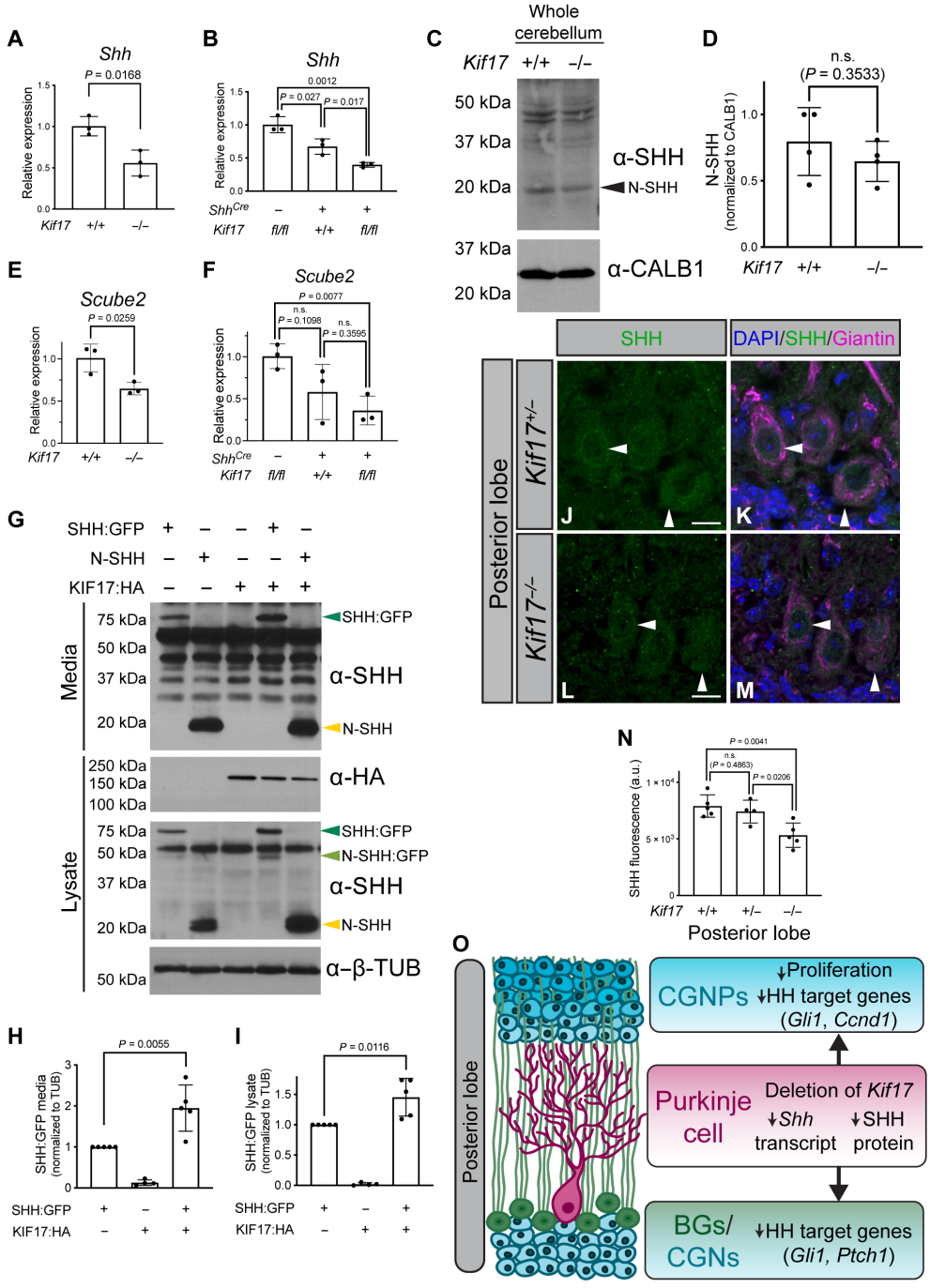


**Fig. 4. KIF17 regulates SHH protein in the developing cerebellum.** RT-qPCR analysis of *Shh* expression (**A** to **B**) in P10 whole cerebella. Western blot detection of SHH, using an N-terminal–directed antibody (**C**) in $Kif17^{+/+}$ and $Kif17^{-/-}$ P10 whole cerebella. Antibody detection of Calbindin (α-CALB1) confirmed equal loading across lanes. Arrowhead denotes secreted N-SHH (19 kDa). Molecular masses (in kilodalton) of protein standards are on the left. Quantitation of N-SHH (**D**) normalized to Calbindin in $Kif17^{+/+}$ and $Kif17^{-/-}$ in P10 whole cerebella. RT-qPCR analysis of *Scube2* expression (**E** and **F**) in P10 whole cerebella. Western blot analysis (**G**) of media and cell lysates from COS-7 cells expressing HA-tagged KIF17 (KIF17:HA), full-length SHH fused to GFP (SHH:GFP), or N-SHH. Blots were incubated with antibodies directed against SHH (α-SHH) and HA (α-HA). Antibody detection of β-tubulin (α–β-TUB) confirmed equal loading across lanes. Arrowheads denote full-length SHH:GFP (68 kDa), N-SHH:GFP (42 kDa), or N-SHH (19 kDa). Molecular masses (in kilodalton) of protein standards are on the left. Quantitation of full-length SHH:GFP in media (**H**) and COS-7 cell lysates (**I**) normalized to β-tubulin. Immunofluorescent detection of SHH using a C-terminal–directed antibody (green; **J** to **M**). DAPI denotes nuclei [blue; (K) and (M)]. Antibody detection of Giantin [magenta; (K) and (M)] in P10 posterior cerebellar sections from $Kif17^{+/-}$ [(J) and (K)] and $Kif17^{-/-}$ [(L) and (M)] mice. Horizontal arrowheads indicate SHH localization to Golgi/ER, while vertical arrowheads denote cytoplasmic localization. Scale bars, 10 μm [(J) and (L)]. Quantitation of SHH fluorescence (**N**) in posterior cerebellar lobes of P10 $Kif17^{+/+}$, $Kif17^{+/-}$, and $Kif17^{-/-}$ mice. Data are means ± SD. Each dot represents an individual animal [(A) and (B) and (D) and (F)], independent experiment [(H) and (I)], or the average of five images per animal (N). *P* values were determined by a two-tailed Student's *t* test. (**O**) Summary of PC-specific *Kif17* deletion on HH ligand production and HH responses in the developing cerebellum.

Given the altered baseline CGNP proliferation, we examined the levels and processing of the HH pathway transcriptional repressor, GLI3, in *Kif17* mutant animals. Western blot analysis of GLI3 full length ($GLI3^{FL}$) and repressor ($GLI3^{R}$) in P10 cerebella (fig. S8B) revealed significant reductions in both $GLI3^{FL}$ and $GLI3^{R}$ in $Kif17^{-/-}$ cerebella (fig. S8, C and D). Furthermore, the ratio of $GLI3^{FL}$ to $GLI3^{R}$ is significantly increased in *Kif17* mutant cerebella (fig. S8E). These data suggest that, similar to other kinesin-2 mutants (*32*), KIF17 regulates GLI3 processing in CGNPs. Together, these data suggest that KIF17 negatively regulates HH signaling in a cell-autonomous fashion within CGNPs, potentially through regulation of GLI3 repressor.

### CGNP-specific *Kif17* deletion results in a cell-autonomous HH gain-of-function phenotype

To directly assess KIF17 function in CGNPs in vivo, we crossed $Kif17^{flox}$ mice to animals carrying *Atoh1Cre* (Fig. 5A), which specifically drives recombination in CGNPs [(*33*) and fig. S9, A to F]. We used RT-qPCR to confirm efficient *Kif17* deletion in $Atoh1Cre;Kif17^{fl/fl}$ cerebella (Fig. 5B and fig. S9G). While *Kif17* expression is reduced in $Atoh1Cre;Kif17^{fl/fl}$ cerebella, *Kif17* expression is unexpectedly increased in $Atoh1Cre;Kif17^{+/+}$ cerebella (fig. S9G). Next, we assessed cerebellar size in $Atoh1Cre;Kif17^{fl/fl}$ animals, which is unchanged compared to control animals (Fig. 5C and fig. S9, H to K). These data are in contrast to *Kif17* germline mutants and PC–specific *Kif17* deletion (cf. Figs. 1S and 3C). While PC dendrite length is not significantly changed in either posterior (lobes VIII to X) or anterior (lobes I to IV) regions of $Atoh1Cre;Kif17^{fl/fl}$ cerebella (Fig. 7D and fig. S9L), EGL thickness is increased, specifically in posterior lobes of $Atoh1Cre;Kif17^{fl/fl}$ cerebella (Fig. 5E and fig. S9M). Notably, increased EGL thickness appears to be due to increased CGNP proliferation (as assessed by the percentage of $EdU^{+}/PAX6^{+}$ cells in the EGL) in both posterior (Fig. 5M) and anterior (fig. S9O) lobes of $Atoh1Cre;Kif17^{fl/fl}$ cerebella. RT-qPCR analysis revealed increased HH target gene expression in $Atoh1Cre;Kif17^{fl/fl}$ cerebella compared to control littermates (Fig. 5, N and O, and fig. S9, P to R). In situ hybridization confirmed that the increase in HH target gene expression is restricted to CGNPs in the posterior lobes, while no changes were observed in HH-responsive BGs and CGNs (Fig. 5T and fig. S9S). Together, these data indicate that CGNP-specific *Kif17* deletion results in increased HH pathway activity and CGNP proliferation, leading to a thicker EGL within posterior lobes of the developing cerebellum.

### CGNP-specific *Kif17* deletion results in reduced GLI protein, increased CGNP proliferation, and elongated primary cilia in vitro

Given that other kinesin-2 motors regulate GLI processing and trafficking, including in the cerebellum (*11*, *12*, *32*), we examined the consequences of CGNP-specific *Kif17* deletion on *Gli* expression and GLI protein levels. *Gli2* and *Gli3* expression are increased in $Atoh1Cre;Kif17^{fl/fl}$ cerebella (fig. S10, A and B), similar to *Gli1*. However, Western blot analysis (Fig. 6A) revealed significantly reduced levels of GLI1 and GLI2 protein (Fig. 6, B and C). Similar to what was observed in $Kif17^{-/-}$ cerebella (cf. fig. S8, B to E), GLI3 full length and GLI3 repressor levels are also reduced (Fig. 7, D and E); further, the ratio of full length ($GLI3^{FL}$) to repressor ($GLI3^{R}$) is increased in *Kif17* mutant CGNPs (Fig. 6F).

We also assessed potential physical interactions between KIF17 and GLI proteins, as previously demonstrated for other Kinesin-2 motors (*13*). Co-immunoprecipitation of epitope-tagged KIF17 (KIF17:HA) and GLI transcription factors (MYC:GLI1, MYC:GLI2, and MYC:GLI3) suggested that KIF17 can indeed physically interact with all three GLI proteins (fig. S10C).

Reduction of both full-length and processed forms of GLI is reminiscent of suppressor of fused (SUFU) loss-of-function cerebella (*34*). In addition, loss of GLI2 or GLI3 leads to loss of ciliary localization of SUFU (*35*). We examined ciliary localization of SUFU [SUFU antibody validated in $Sufu^{-/-}$ MEFs (*36*) (fig. S10, D to I)] in control and $Atoh1Cre;Kif17^{fl/fl}$ CGNPs in response to SAG (fig. S10, J to V). We detected SUFU at the tips of cilia in both $Kif17^{fl/fl}$ and $Atoh1Cre;Kif17^{fl/fl}$ CGNPs, albeit a lower percentage of $SUFU^{+}$ cilia was observed in $Atoh1Cre;Kif17^{fl/fl}$ CGNPs. Together, these data suggest that KIF17 affects GLI stability and/or processing, potentially through regulating SUFU-GLI interactions.

We noted that *Atoh1* expression is increased in animals with CGNP-specific *Kif17* deletion (fig. S11A); previous work demonstrated that ATOH1 promotes ciliogenesis and maintains CGNP responsiveness to HH (*37*). However, analysis of CGNP primary cilia length in $Atoh1Cre;Kif17^{fl/fl}$ P10 cerebella revealed no significant change in vivo ($P = 0.4534$ for posterior lobes and $P = 0.0886$ for anterior lobes; fig. S11, B and C). In contrast, when we examined primary ciliary length in SAG-treated CGNPs in vitro, we found that CGNPs lacking *Kif17* display increased ciliary length (Fig. 6, G to L), with an average ciliary length of 1.46 μm (compared to 1.1 μm in control animals); notably, some primary cilia reached lengths of 5 μm (Fig. 6K).

Because HH signaling also regulates cilia length (*38*) and ciliogenesis (*39*), we investigated whether increased ciliary length was a cause or a consequence of HH pathway activity. We antagonized HH signaling in vitro by adding bone morphogenetic protein (BMP) ligands, either BMP2, which has been previously shown to antagonize SHH-induced CGNP proliferation (*40*) or BMP10, which is significantly up-regulated in $Kif17^{-/-}$ cerebella (fig. S11D). While *Bmp10* expression is up-regulated in $Kif17^{-/-}$ whole cerebella, it is not altered in $Kif17^{-/-}$ CGNPs (fig. S11D). These data are consistent with the observed differences in $Kif17^{-/-}$ CGNP proliferation in vivo and in vitro (cf. Fig. 2 and fig. S7, A to G) and suggest that there are multiple BMP sources in the cerebellum. *Bmp10* is also expressed in PCs and CGNs in rodent cerebella [Allen Institute Developing Brain Atlas, (*41*)]. Notably, both BMP2 and BMP10 effectively attenuate HH-mediated CGNP proliferation in both $Kif17^{fl/fl}$ and $Atoh1Cre;Kif17^{fl/fl}$ cultures (Fig. 6L and fig. S11, E to M). However, BMP2 and BMP10 treatment reduced ciliary length specifically in $Atoh1Cre;Kif17^{fl/fl}$ CGNPs (Fig. 6, M to S, and fig. S11N), resulting in average ciliary lengths of 1.18 μm (BMP2) and 1.17 μm (BMP10). Together, these data suggest that high levels of HH pathway activation in *Kif17* mutant CGNPs result in increased ciliary length, which can be attenuated by BMP signaling.

## DISCUSSION

In this study, we investigated a role for the kinesin-2 motor KIF17 in HH-dependent cerebellar development. Our work revealed that *Kif17* is expressed in both SHH-producing PCs and SHH-responsive CGNPs. PC–specific *Kif17* deletion and germline *Kif17* deletion similarly result in reduced EGL thickness due to reduced HH target gene expression and decreased CGNP proliferation. Conversely, CGNP-specific *Kif17* deletion increased EGL thickness due to increased HH target gene expression and increased CGNP proliferation (Fig. 7). This work

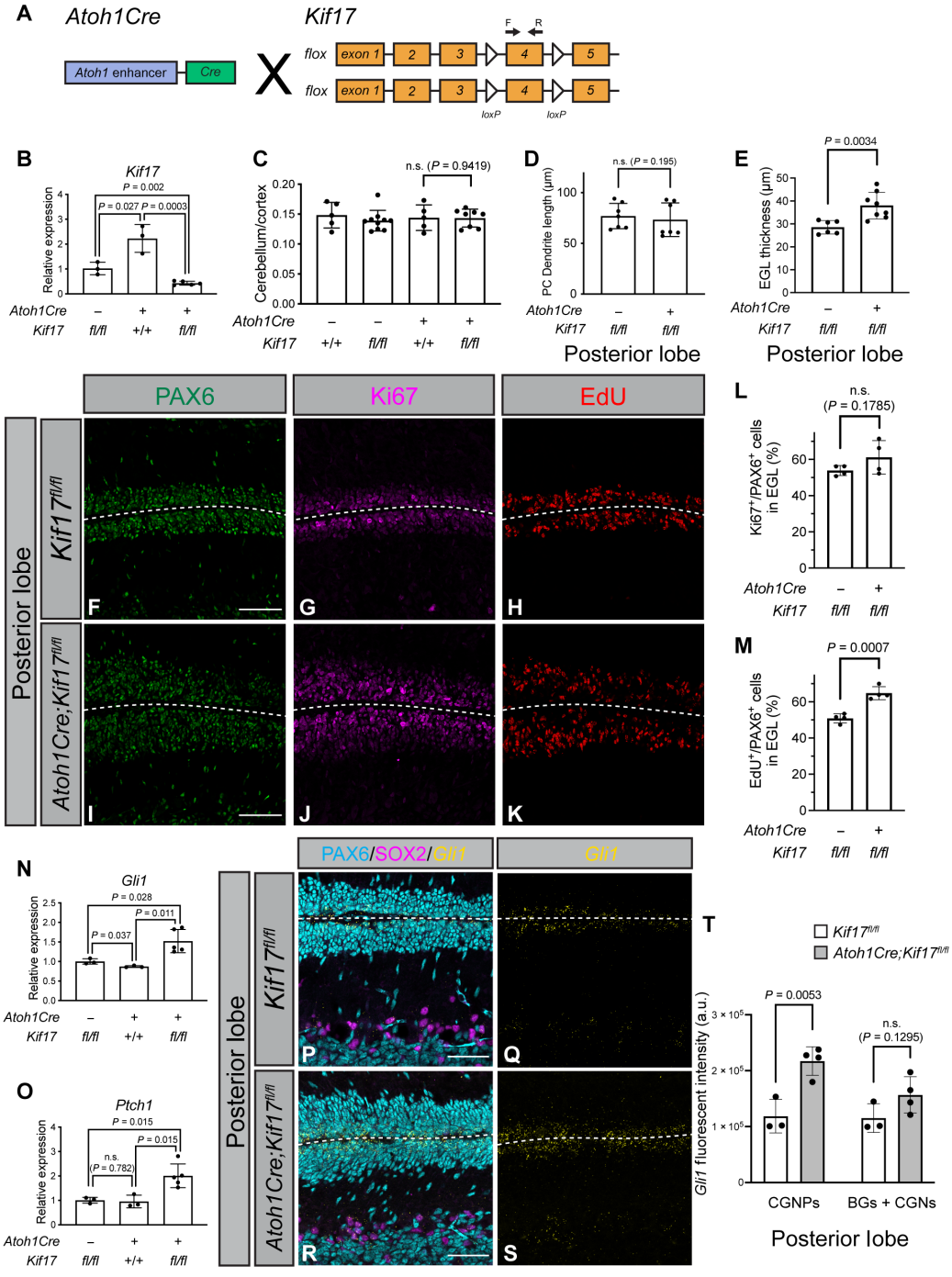


**Fig. 5. CGNP-specific *Kif17* deletion results in a cell-autonomous HH gain-of-function phenotype.** (**A**) Schematic representing conditional *Kif17* deletion within CGNPs using *Atoh1Cre*. Arrows above exon 4 denote qPCR primers. Relative *Kif17* expression (**B**) measured by RT-qPCR in P10 cerebella from *Kif17*$^{fl/fl}$, *Atoh1Cre;Kif17*$^{+/+}$ and *Atoh1Cre;Kif17*$^{fl/fl}$ mice. Cerebellar weights normalized to cortical weights (**C**) in P10 control and CGNP-specific *Kif17* deletion mice. Quantitation of PC dendrite length (**D**) and EGL (**E**) thickness in posterior lobes of *Kif17*$^{fl/fl}$ and *Atoh1Cre;Kif17*$^{fl/fl}$ P10 cerebella. Analysis of in vivo CGNP proliferation by immunofluorescence in *Kif17*$^{fl/fl}$ (**F** to **H**) and *Atoh1Cre;Kif17*$^{fl/fl}$ (**I** to **K**) P10 cerebella. Antibody detection of PAX6 [green; (F) and (I)] and Ki67 [magenta; (G) and (J)]. Fluorescent azide detection of EdU [red; (H) and (K)]. Scale bars, 50 μm [(F) and (I)]. Percentage of Ki67$^+$/PAX6$^+$ (**L**) and EdU$^+$/PAX6$^+$ (**M**) cells within the posterior cerebellar lobes of *Kif17*$^{fl/fl}$ and *Atoh1Cre;Kif17*$^{fl/fl}$ P10 mice. Relative *Gli1* (**N**) and *Ptch1* (**O**) expression measured by RT-qPCR in *Kif17*$^{fl/fl}$, *Atoh1Cre;Kif17*$^{+/+}$ and *Atoh1Cre;Kif17*$^{fl/fl}$ P10 whole cerebella. Fluorescent in situ *Gli1* detection (yellow; **P** to **S**) with immunofluorescent detection of PAX6 to mark CGNPs and CGNs [cyan; (P) and (R)] and SOX2 to identify BG [magenta; (P) and (R)] within posterior cerebellar lobes of P10 *Kif17*$^{fl/fl}$ and *Atoh1Cre;Kif17*$^{fl/fl}$ littermates. Scale bars, 50 μm [(P) and (R)]. Quantitation of fluorescent intensity (integrated density) of *Gli1* puncta (**T**) within either CGNPs or BGs and CGNs (BGs + CGNs) in posterior cerebellar lobes of P10 *Kif17*$^{fl/fl}$ and *Atoh1Cre;Kif17*$^{fl/fl}$ mice. Data are means ± SD. Each dot represents an individual animal [(B) to (E) and (N) and (O)] or the average of five images per animal [(L) and (M) and (T)]. *P* values were determined by a two-tailed Student's *t* test. Dashed lines separate EGLs.

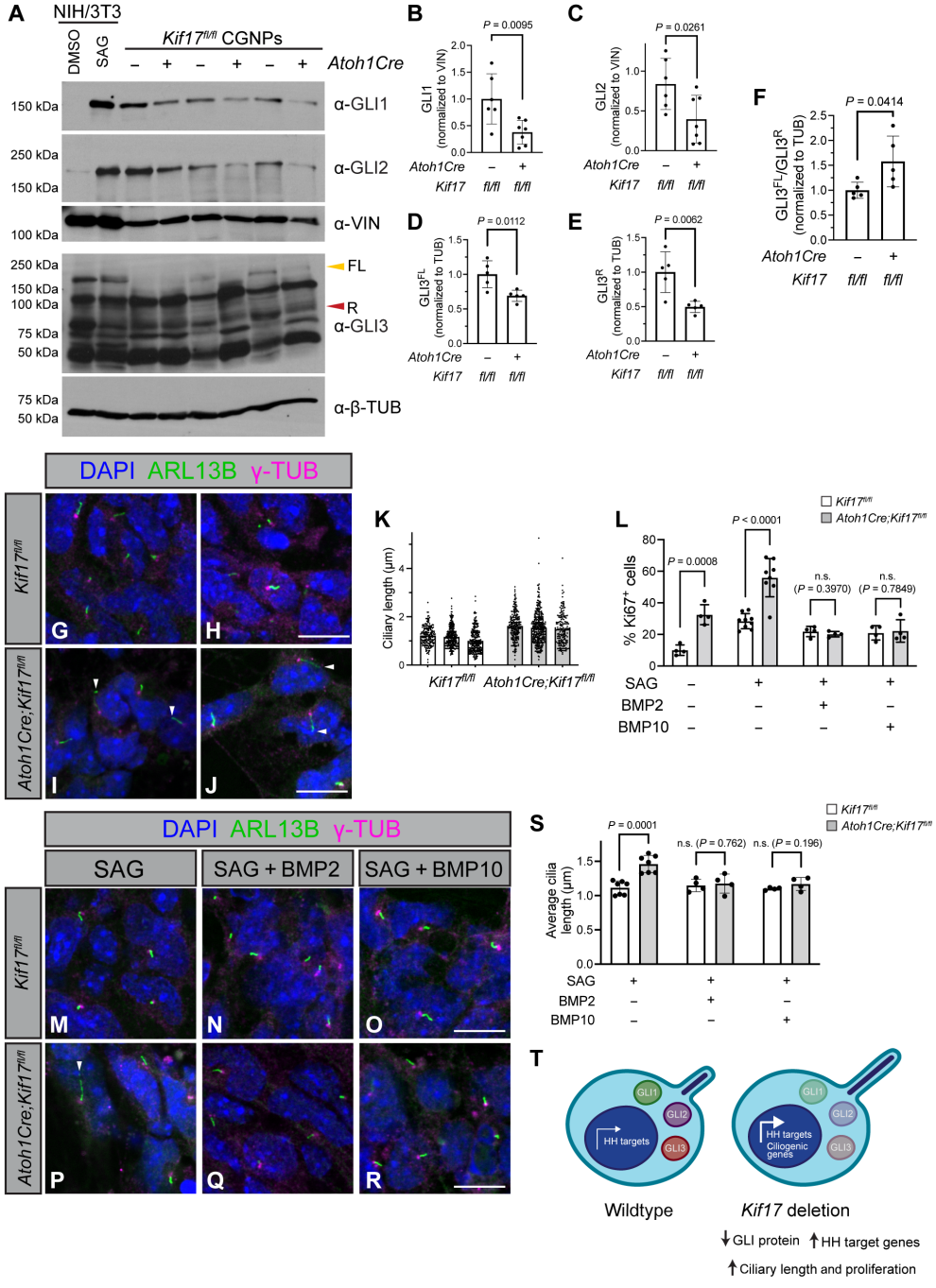


**Fig. 6. CGNP-specific *Kif17* deletion results in reduced GLI protein, increased CGNP proliferation, and elongated primary cilia.** Western blot detection (**A**) of GLIs (α-GLI1, α-GLI2, and α-GLI3) in NIH/3T3 cells and purified CGNPs isolated from *Kif17*$^{fl/fl}$ and *Atoh1Cre;Kif17*$^{fl/fl}$ littermates. Antibody detection of Vinculin (α-VIN) or β-tubulin (α–β-TUB) confirmed equal loading across lanes. Yellow arrowhead denotes full-length GLI3 (FL; 180 kDa), and red arrowhead indicates GLI3 repressor (R, 83 kDa). Molecular masses (in kilodalton) of protein standards are on the left. GLI1 (**B**) and GLI2 (**C**) quantitation, normalized to Vinculin. GLI3$^{FL}$ (**D**) and GLI3$^{R}$ (**E**) levels, normalized to β-tubulin. Ratio of GLI3$^{FL}$ to GLI3$^{R}$ (**F**) in *Kif17*$^{fl/fl}$ and *Atoh1Cre;Kif17*$^{fl/fl}$ CGNPs, normalized to β-tubulin. Visualization of primary cilia (**G** to **J**) from *Kif17*$^{fl/fl}$ [(G) and (H)] and *Atoh1Cre;Kif17*$^{fl/fl}$ [(I) and (J)] CGNP cultures treated with SAG. Antibody detection of ARL13B (green) and γ-tubulin (γ-TUB; magenta) denote axonemes and basal bodies, respectively; nuclei are identified with DAPI (blue). Scale bars, 10 μm [(H) and (J)]. Ciliary length (**K**) quantitation of CGNPs from three representative cultures of *Kif17*$^{fl/fl}$ and *Atoh1Cre;Kif17*$^{fl/fl}$ littermates. Each dot represents an individual cilium. Percentages of Ki67$^{+}$ (**L**) cells in CGNP cultures from P8 *Kif17*$^{fl/fl}$ and *Atoh1Cre;Kif17*$^{fl/fl}$ littermates. Cells were treated with vehicle dimethyl sulfoxide (DMSO) or SAG, with or without BMP2 or BMP10. Visualization of primary cilia from *Kif17*$^{fl/fl}$ (**M** to **O**) and *Atoh1Cre;Kif17*$^{fl/fl}$ (**P** to **R**) CGNP cultures treated with SAG and BMP. Antibody detection of ARL13B (green) and γ-tubulin (magenta) label axonemes and basal bodies, respectively; nuclei are identified with DAPI (blue). Scale bars, 10 μm [(O) and (R)]. Average CGNP ciliary length (**S**) from *Kif17*$^{fl/fl}$ and *Atoh1Cre;Kif17*$^{fl/fl}$ littermates; each dot represents the average length of an individual culture. Data are mean ± SD. *P* values were determined by a two-tailed Student's *t* test. (**T**) Summary of CGNP-specific *Kif17* deletion on GLIs, CGNP proliferation, and primary cilia length.

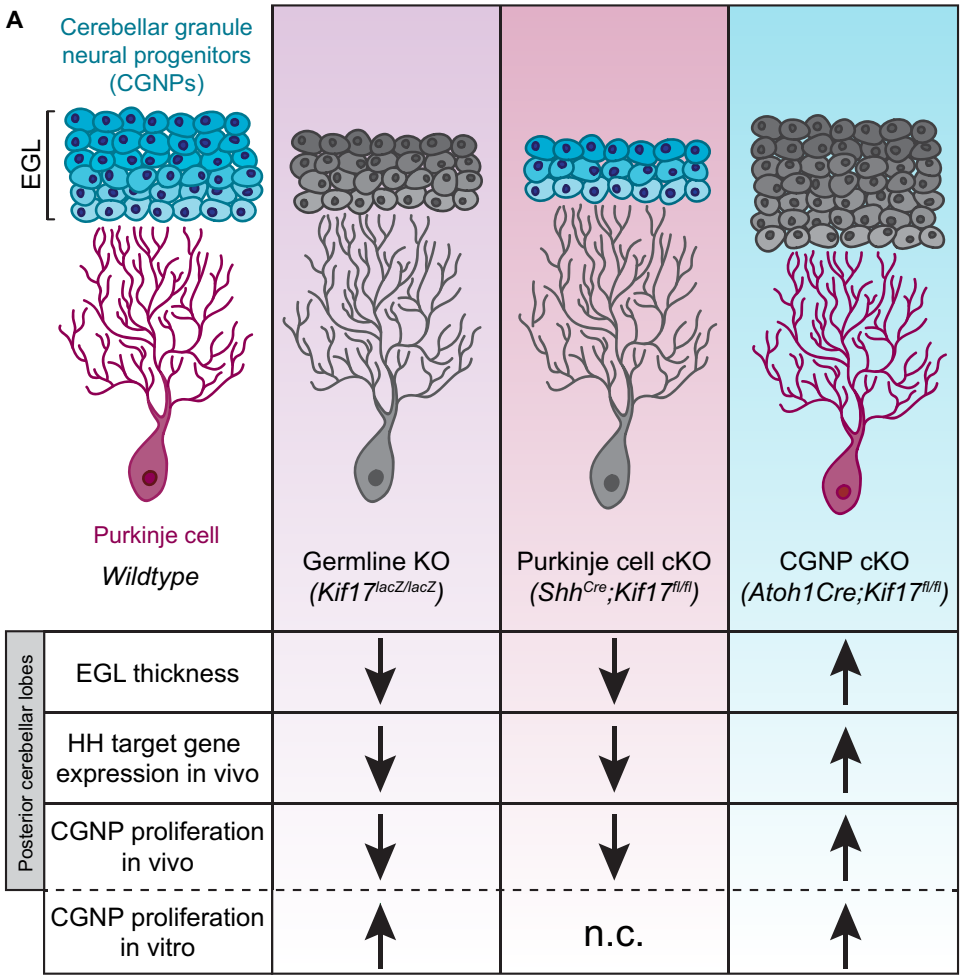


**Fig. 7. KIF17 has dual and opposing roles in HH signaling in the developing cerebella.** (**A**) Schematic demonstrating the consequences of KIF17 deletion on cerebellar development, in particular the posterior lobes. Germline or PC–specific *Kif17* deletion (magenta) results in a HH loss-of-function phenotype in vivo, while CGNP-specific *Kif17* deletion yields a HH gain-of-function phenotype (cyan). Notably, germline *Kif17* deletion results in increased CGNP proliferation in vitro, similar to CGNP-specific *Kif17* deletion both in vivo and in vitro.

identifies dual and opposing roles for KIF17 in HH-dependent cerebellar development—first, as a positive regulator of HH signaling through regulation of SHH protein levels within PC, and second, as a negative regulator of HH signaling through regulation of GLI transcription factors in CGNPs.

### KIF17 function in SHH-producing PCs

Here, we demonstrated that KIF17 is required in PCs to mediate proper HH-dependent cerebellar development and that KIF17 regulates SHH protein levels within PCs. Specifically, we visualized intracellular SHH using a C-terminal antibody, which revealed reduced SHH protein in *Kif17* mutant cerebella, both within the presumed endoplasmic reticulum/Golgi apparatus and more broadly within PC cell bodies. Notably, SHH is translated as a 45-kDa precursor protein, which undergoes autocatalytic cleavage into a 19-kDa N-terminal fragment and 25-kDa C-terminal fragment (*42*–*44*). The N-terminal fragment is dually lipidated with cholesterol at the C terminus and palmitate at the N terminus to produce active ligand [reviewed in (*45*)]. While the 25-kDa C-terminal SHH fragment does not transduce HH signaling, the C-terminal HH fragment does target N-HH to axons and growth cones in the developing retina of *Drosophila melanogaster* (*46*). One model for KIF17 action in PCs is the transport of SHH-containing vesicles along microtubules to distinct locations within these cells. This model has precedence with a previously described role for KIF17 in the vesicular trafficking of NR2B in the hippocampus (*17*, *25*). Furthermore, this is consistent with the reduced levels of SHH protein in *Kif17* mutants, as NR2B levels are also reduced when its vesicular trafficking is disrupted in *Kif17* mutants. This model is also consistent with the results from KIF17 gain-of-function experiments demonstrating increased intracellular SHH protein accumulation (this study). Notably, PCs contain primary cilia (*27*). It remains to be determined whether KIF17-mediated regulation of SHH is cilia dependent. Furthermore, we cannot rule out similar trafficking-related effects of KIF17 on other HH pathway components, such as SCUBE2 and DISP, both of which regulate SHH protein release from cell surfaces. We also cannot distinguish between KIF17-mediated effects on SHH trafficking versus potential impacts on SHH protein stability. Distinguishing

between these possibilities would require robust methods to culture PCs ex vivo, which are currently lacking. Last, while we observed a reduction in the total number of PCs per section, we did not observe any gross morphological changes or altered density of PCs with *Kif17* deletion. In addition, while we did not observe a significant difference in PC ciliary length with *Kif17* deletion, we cannot rule out a subtle defect in cilia structure that could be resolved with electron microscopy. Future studies assessing PC specification, proliferation, and survival will reveal greater insight into KIF17 function during cerebellar development. Along these lines, it remains to be explored whether PC function or the secretion of other PC–derived ligands, such as insulin-like growth factor 1, could also be affected by *Kif17* deletion.

### KIF17 regulation of GLIs in CGNPs

In addition to a non–cell-autonomous role for KIF17 in PCs, we also established a cell autonomous role for KIF17 in CGNPs, where *Kif17* deletion results in a HH gain-of-function phenotype—increased CGNP proliferation and up-regulation of several HH target genes. CGNP-specific *Kif17* deletion results in reduced protein levels of all three HH transcriptional effectors, GLI1, GLI2, and GLI3. Previous work established GLI1 and GLI2 as transcriptional activators in the developing cerebellum, where *Gli2* deletion results in a HH loss-of-function phenotype (*4*, *6*). Given these roles for GLI1 and GLI2, we were surprised to find that CGNP-specific *Kif17* deletion results in a HH gain-of-function phenotype. However, the concomitant loss of GLI3 repressor in *Kif17* mutant CGNPs suggests that GLI repressor function is a significant mediator of CGNP proliferation. Notably, reduction of GLI activator and repressor protein is consistent with previous work where cerebellar-specific *Sufu* deletion also results in increased CGNP proliferation (*34*). GLI3 also acts during early embryonic cerebellar development in mesencephalon and rhombomere 1 patterning through the regulation of *Fgf8* expression (*47*). Together, these data suggest that KIF17 in CGNPs promotes GLI3 repressor formation to restrict proliferation in the postnatal cerebellum, consistent with previous work demonstrating central roles for other kinesin-2 motors in GLI processing (*11*, *32*, *48*).

GLIs require primary cilia for proper processing and transcriptional activity [reviewed in (*8*)]. Furthermore studies have established ciliary tip localization of KIF17 (*49*), similar to GLI transcription factor localization during HH activation (*50*, *51*). One model for KIF17 regulation of GLI protein levels in CGNPs is through ciliary trafficking or localization. Notably, this is consistent with recent work demonstrating that GLI interactions with KIF7 promote ciliary localization (*52*). Unfortunately, the lack of suitable KIF17 antibodies precludes rigorous testing of this hypothesis. Other possible roles for KIF17 in CGNPs include the regulation of GLI trafficking and stability as well as interactions with other ciliary proteins that regulate GLI processing, such as SUFU, KIF7, or PKA (*53*–*55*). We observe that SUFU does localize to the tips of cilia with the loss of KIF17, although at a reduced proportion. This may be due to KIF17 interactions with SUFU or due to the reduced abundance of GLI transcription factors. Previous literature demonstrates that the loss of GLI2 or GLI3 results in a loss of ciliary SUFU (*35*).

### Kinesin motors and HH signaling

While previous studies have explored the requirements for kinesin and dynein motors in HH-responding cells [reviewed in (*8*)], the current study highlights a novel role for kinesin-2 motors in HH-producing cells, complementing recent work examining KIF3B and SHH in the developing limb bud (*56*). Notably, individual *Kif17* deletion in PCs is sufficient to result in a HH loss-of-function phenotype. It remains to be seen whether other kinesin-2 motors also function in SHH-producing cells in the cerebellum. Another outstanding question is whether KIF17 functions in HH-producing cells in other tissues. Specifically, the subgranular zone of the hippocampus and subventricular zone rely on proper HH signaling for neurogenesis (*57*–*60*). While KIF17 has a well-defined role in NR2B trafficking in the hippocampus (*17*, *25*), the potential contribution of KIF17 to HH signaling in the hippocampus has not yet been examined.

In addition to its neural-specific contributions, KIF17 has several described functions in the testes, although loss-of-function studies have yet to be performed (*61*–*65*). Desert HH (DHH) is expressed in Sertoli cells, and *Dhh* deletion results in a loss of HH-responsive Leydig cells (*66*). While we did not observe infertility in *Kif17* mutant mice, it will be of interest to investigate the consequences of *Kif17* deletion on HH-dependent spermatogenesis. Future studies investigating the contribution of other kinesin-2 motors, particularly KIF3A/KIF3B, in HH-producing cells (e.g., in the notochord or zone of polarizing activity) will be of high interest. Last, this work raises the question of potential contributions from KIF3C, another accessory kinesin-2 motor, to HH signal transduction.

## MATERIALS AND METHODS

### Animal models

$Kif17^{lacZ}$ germline mutant mice have been previously described (*22*). These mice were maintained on two different congenic C57BL/6J and 129S4/SvJaeJ backgrounds after backcrossing for at least 10 generations. $Kif17^{fl}$ animals carrying *Kif17* conditional alleles were generated from the initial knock-in allele from EUCOMM through crossing $Kif17^{tm1A}$ animals to ubiquitous Flippase mice obtained from the Jackson Laboratory [strain 011065, (*67*)] to generate $Kif17^{tm1C}$/$Kif17^{flox}$ mice. These mice were maintained on a congenic C57BL/6J background. *Atoh1Cre* animals were obtained from the Jackson Laboratory [strain 011104, (*33*)] and maintained on a C57BL/6J background. Mice carrying the $Shh^{Cre}$ allele [strain 005622] were provided by D. Gumucio and previously described (*26*). These mice were backcrossed for at least 10 generations to C57BL/6J animals to create a congenic line. All animal procedures were reviews and approved by the Institutional Animal Care and Use Committee at the University of Michigan, USA. Experiments performed in this paper were completed with littermate controls.

### Whole-mount X-GAL staining

Postnatal cerebella were dissected in 1X phosphate-buffered saline (PBS) (pH 7.4) and cut in half with a razor before fixation (1% formaldehyde, 0.2% glutaraldehyde, 2 mM $MgCl_2$, 5 mM EGTA, and 0.02% NP-40) on ice for 20 min. After fixation, the cerebella were washed three times for 5 min with 1X PBS (pH 7.4) on a rocking platform. β-GAL activity was detected with X-gal staining solution [5 mM $K_3Fe(CN)_6$, 5 mM $K_4Fe(CN)_6$, 2 mM $MgCl_2$, 0.01% Na deoxycholate, 0.02% NP-40, and X-gal (1 mg/ml)]. The signal was developed for 24 hours at 37°C, changing the staining solution after 12 hours. After staining, cerebella were washed three times for 5 min with 1X PBS (pH 7.4) and post-fixed in 4% paraformaldehyde for 30 min at room temperature on a rocking platform, followed by three 5-min washes in 1X PBS (pH 7.4). Cerebella were photographed using a Nikon SMZ1500 microscope and stored in 1X PBS (pH 7.4).

### Section immunofluorescence

Section immunofluorescence was performed as described in (*68*). Briefly, cerebella were dissected in 1X PBS (pH 7.4) and cut in half using a razor. For all experiments except for β-GAL and SHH visualization, cerebella were fixed with 4% paraformaldehyde (Electron Microscopy Sciences) for 1 hour on ice. For β-GAL immunofluorescence, cerebella were fixed (1% formaldehyde, 0.2% glutaraldehyde, 2 mM $MgCl_2$, 5 mM EGTA, and 0.02% NP-40) on ice for 20 min. For SHH visualization, cerebella were fixed in Sainte Marie's solution (95% ethanol and 1% acetic acid) at 4°C on a rocking platform for 24 hours. Following fixation, cerebella were washed three times for 5 min with 1X PBS (pH 7.4) on a rocking platform and cryoprotected overnight in 1X PBS + 30% sucrose on a rocking platform. Then, cerebella were washed three times for 1 hour in 50% optimal cutting temperature (OCT) compound (Thermo Fisher Scientific, 23-730-571) before embedding in 100% OCT compound. Sections were collected on a Leica CM1950 cryostat at 12-μm thickness for all experiments, except for SHH visualization, which were sectioned at 9-μm thickness. Slides were then washed three times for 5 min with 1X PBS (pH 7.4). For mouse primary antibodies, citric acid antigen retrieval [10 mM citric acid + 0.5% Tween 20 (pH 6.0)] at 92°C for 10 min was performed before primary antibody incubation. Primary antibodies were diluted in blocking buffer (3% bovine serum albumin, 1% heat-inactivated sheep serum, and 0.1% Triton X-100) and incubated overnight at 4°C in a humidified chamber. After primary antibody incubation, slides were washed three times for 10 min with 1X $PBST^X$ [1X PBS + 0.1% Triton X-100 (pH 7.4)]. Secondary antibodies were diluted in blocking buffer and incubated for 1 hour at room temperature, followed by three for 5-min washes in 1X $PBST^X$. Nuclei were labeled using 4′,6-diamidino-2-phenylindole (DAPI) (0.5 μg/ml in blocking buffer) for 10 min and washed twice with 1X PBS. Coverslips were mounted using Immu-Mount aqueous mounting medium (Thermo Fisher Scientific, 9990412). Images were taken on a Leica SP5X upright confocal (two photon). A list of all the primary and secondary antibodies and their working concentrations is provided in table S1.

### Fluorescent in situ hybridization

Cerebella were dissected in 1X PBS (pH 7.4) and cut in half using a razor. Cerebella were fixed with 10% neutral-buffered formalin (Thermo Fisher Scientific, 245-685) on a rocking platform at room temperature for 24 hours. Following fixation, cerebella were washed three times for 5 min with 1X $PBST^X$ on a rocking platform and cryoprotected overnight in 1X PBS + 30% sucrose on a rocking platform. Cerebella were then washed three times for 1 hour with 50% OCT compound before embedding in 100% OCT compound. Sections were collected on a Leica CM1950 cryostat at 12-μm thickness. Slides were processed using RNAscope Multiplex Fluorescent Detection kit (ACD, 323110) using a protocol adapted from (Holloway, 2021). Before probe hybridization, samples underwent antigen retrieval for 15 min and treated with Protease Plus (ACD, 322381) for 5 min. Probes used here were *Mm-Gli1* (ACD, 311001) and *E.coli-lacZ* (ACD, 313451). After probe detection, slides were subsequently stained using the above-described section immunofluorescence protocol.

### RT-qPCR

Cerebella were dissected in 1X PBS, and RNA was isolated using the PureLink RNA Mini Kit (Thermo Fisher Scientific, 12183025). Following isolation, 2 μg of RNA was used to generate cDNA libraries using a High-Capacity cDNA reverse transcription kit (Applied Biosystems, 4368814). RT-qPCR was performed using PowerUP SYBR Green Master Mix (Applied Biosystems, A25742) in a QuantStudio 3 Real-Time PCR System (Applied Biosystems). Primers used here can be found in table S2. Gene expression was normalized to *Gapdh*, except for Fig. 3B, where expression was normalized to *Calb1*, and relative expression analyses were performed using the $2^{(-ddCT)}$ method. For RT-qPCR analysis, biological replicates were analyzed in triplicate.

### Weight analyses

For weight measurements, the date litters were born were noted as P0 and were dissected on P10. Pups were first weighed and then placed on ice briefly before decapitation. The cortices and cerebella were dissected in 1X PBS (pH 7.4). To weigh cortices and cerebella, a specimen jar was first filled with PBS on an analytical scale. The tissue was transferred with forceps to the specimen jar, and its weight was recorded. Genotyping samples were taken after dissection, allowing the weights to be recorded without prior knowledge of the genotype.

### Hematoxylin and eosin staining and cerebellar area quantitation

Tissue sections were washed once for 5 min in water, stained with hematoxylin for 5 min, then rinsed in water and 1X PBS (pH 7.4) for 10 s. Slides were counterstained with eosin solution, rinsed in water, and dehydrated in an ethanol and xylene series (once for 1 min in 95% ethanol, twice for 2 min in 100% ethanol, and twice for 2 min in 100% xylene). Slides were mounted using Cytoseal 60 mounting media and imaged on a Nikon SMZ1500 stereomicroscope. For cerebellar area quantitation, we analyzed two to five sections per animal and a minimum of 2 animals per genotype. Cerebellar area measurements were collected using the area measure function on ImageJ.

### EGL and PC dendrite quantitation

To measure the thickness of the EGL and PC dendrites, ImageJ software was used. Images were first blinded before measuring. For EGL thickness, the area was divided by the length of the EGL. For PC dendrite length, measurements were taken just below the bottommost nuclei in the EGL to the center of PC nuclei within the molecular layer. For each animal, at least three images were acquired in the posterior lobes and an additional three images in the anterior lobes.

### EdU incorporation assay (in vivo)

On P9, pups were intraperitoneally injected with EdU (100 mg/kg; Invitrogen, A10044), dissolved in 1X PBS (pH 7.4). Twenty-four later, cerebella were dissected and processed for section immunofluorescence as described above. Before primary antibody incubation, EdU incorporation was visualized with an azide staining solution [100 mM tris-HCl (pH 8.3), 0.5 mM $CuSO_4$, 50 mM ascorbic acid, 50 μM Alexa Fluor 555 azide, and triethylammonium salt (Thermo Fisher Scientific, A20012)] for 30 min at room temperature. Sections were then washed three times for 10 min in $PBST^X$ [1X PBS + 0.1% Triton X-100 (pH 7.4)], followed by immunofluorescence staining as described above.

### Section digoxigenin in situ hybridization

Section digoxigenin in situ hybridization was performed as previously described (*68*, *69*). First, cerebella were dissected in 1X PBS

(pH 7.4) and fixed for 24 hours with 4% paraformaldehyde at 4°C on rocking platform. After fixation, cerebella were washed three times for 5 min with 1X PBST$^{W}$ [1X PBS + 0.1% Tween 20 (pH 7.4)] and cryoprotected with 1X PBS + 30% sucrose overnight on a rocking platform. The next day, cerebella were subjected to three 1-hour washes with 50% OCT before embedding in 100% OCT. Cerebella were sectioned on Leica CM1950 cryostat at 20-μm-thick sections. Probe hybridization was performed with the indicated digoxigenin probes at a concentration of 1 ng/μl overnight at 70°C. The sections were incubated in alkaline phosphatase (AP)-conjugated anti-DIG antibody (table S1). AP–anti-DIG was visualized with BM Purple (Roche, 11442074001), and signal was developed for 4 hours at 37°C. After the signal was developed, development was stopped with three 5-min washes with 1X PBS (pH 4.5). Sections were post-fixed in 4% paraformaldehyde + 0.2% glutaraldehyde for 30 min and then washed three times for 5 min in 1X PBS (pH 7.4). Sections were dried with 70% ethanol wash before drying at 60°C for 10 min. Coverslips were mounted using Glycergel (Dako, C056330-2) pre-heated to 60°C. Images were taken on a Nikon SMZ1500 microscope.

### Western blot analysis

#### *For cerebellar lysates*

For cerebellar lysates, cerebella were dissected in 1X PBS (pH 7.4) and lysed in radioimmunoprecipitation assay buffer [50 mM tris-HCl (pH 7.2), 150 mM NaCl, 0.1% Triton X-100, 1% sodium deoxycholate, and 5 mM EDTA] containing protease inhibitor (Roche, 11836153001) and 1 mM phenylmethylsulfonyl fluoride (PMSF; Sigma-Aldrich, 10837091001). Extracts were cleared by centrifugation at 21,130 rcf for 10 min at 4°C. Total protein concentration was determined with the Pierce BCA Protein Assay Kit (Thermo Fisher Scientific), using 50 μg of cerebellar lysate for each sample. Lysates were mixed with 6X Laemmli buffer and denatured at 95°C for 10 min. Protein was separated by SDS–polyacrylamide gel electrophoresis (SDS-PAGE) (5% separating gel for GLI1 and GLI2, 6.25% for GLI3, and 12% for SHH) and transferred onto Immuno-Blot polyvinylidene difluoride (PVDF) membranes (Bio-Rad) at 100 v for 100 min on ice. For most blots, primary antibodies were diluted in blocking buffer [bovine serum albumin (30 g/liter) with 0.2% $NaN_3$ in 1X TBST (tris-buffered saline and 0.5% Tween 20 (pH 7.4)]. Blots were incubated with primary antibodies overnight at 4°C on a rocking platform. For detecting SHH, the primary antibody was diluted in 1X TBST, and blots were incubated with primary antibody for 1 hour at room temperature on a rocking platform. All primary antibodies and concentrations used can be found in table S1. After incubation with primary antibody, blots were washed three times for 10 min in 1X TBST. Peroxidase-conjugated secondary antibodies (table S1) were diluted in blocking buffer, and blots were incubated with secondary antibodies for 1 hour at room temperature on a rocking platform. After secondary incubation, blots were washed four times for 10 min in 1X TBST, following incubation with Amersham ECL Prime Western Blotting Detecting Reagent (GE Healthcare, RPN2232) for 2 min, then exposed to HyBlot CL autoradiography film (Thermo Fisher Scientific, NC9556985), and developed using a Konica Minolta SRX-101A medical film processor. Relative levels were obtained by taking the integrated density value of each band, subtracting the background of the lane, and normalizing to the integrated density of housekeeping protein (CALB1, VINCULIN, and β-TUB) minus the background of the lane.

For COS-7 overexpression lysates, COS-7 cells were transiently transfected with the relevant DNA constructs using Lipofectamine 2000 (Invitrogen, catalog number 11668). The medium was collected, and cells were lysed 48 hours after transfection in Hepes lysis buffer [25 mM Hepes (pH 7.4), 115 mM KOAc, 5 mM NaOAc, 5 mM $MgCl_2$, 0.5 mM EGTA, and 1% Triton X-100] containing protease inhibitor (Roche, catalog number 11836153001) and 1 mM PMSF (Sigma-Aldrich, 10837091001). Culture media and extracts were cleared by centrifugation at 15,000 rpm for 10 min at 4°C. Total protein concentration was determined for cell lysates with the Pierce BCA Protein Assay Kit (Thermo Fisher Scientific) using 50 μg of cell lysate for each sample. Collected culture medium was diluted 1:5 in Hepes lysis buffer before mixing with 6X Laemmli buffer and denatured at 95°C for 10 min. Protein was separated by SDS-PAGE using 12% gels and transferred onto Immuno-Blot PVDF membranes (Bio-Rad). Membranes with cell lysates were treated identical to cerebellar lysates, as described above.

### Tamoxifen induction

To conditionally delete *Shh* in *Shh*$^{CreER/lacZ}$ mice, neonatal pups were injected intraperitoneally with tamoxifen (50 mg/kg; Sigma-Aldrich, T5648-1G) dissolved in corn oil once daily on P7, P8, and P9. On P10, cerebella were collected and processed for section immunofluorescence described above.

### CGNP cultures

The protocol was adapted from (*31*). P8 animals were anesthetized on ice briefly before decapitation. Cerebella were dissected in 1X PBS (pH 7.4) and placed in Hibernate-A media (BrainBits, Hibernate-A). Tissue was then washed once with 1X PBS (pH 7.4). Cerebella were incubated in digestion media [0.25% Trypsin-EDTA (Gibco, ILT25200056) + deoxyribonuclease I (1 mg/ml; Roche, 10104159001)] for 5 min at 37°C, followed by trituration with a P1000 pipette, and subsequent incubation for 15 min at 37°C, shaking the dish every 5 min. After digestion, the pieces of tissue were further broken up with a P1000 pipette and transferred to a conical containing isolation media [Dulbecco's modified Eagle medium (Gibco, 11965-092) + 10% calf bovine serum {American Type Culture Collection (ATCC), 50-189-025NP] + 1× penicillin-streptomycin-glutamine (Gibco, 10378016)}. The digested tissue was spun down 800 rcf for 8 min to pellet the cells. Digestion medium was removed, and the pellet was washed with twice more isolation media. The pellet was fully resuspended in isolation media and passed through a 70-μm cell strainer. Single-cell suspensions were spun down and resuspended in 1 ml of isolation media, which was then added to the top of a 30%/60% Percoll gradient (Sigma-Aldrich/Cytiva, P1644) before spinning at 800 rcf for 20 min. Initially, 100% Percoll was diluted with 10X PBS to make 90% Percoll. For 60% Percoll, 90% Percoll was diluted in L15 complete media [Leibovitz's L-15 Medium without phenol red (Gibco, 21083027) + 10% calf bovine serum (ATCC, 50-189-025NP) + 1× penicillin-streptomycin-glutamine (Gibco, 10378016)]. For 30% Percoll, 90% Percoll was diluted in isolation media. CGNPs were isolated from the 30%/60% Percoll interphase and washed with isolation media. Last, CGNPs were resuspended in neuronal media [Neurobasal media (Gibco, 21103049) + 1% calf bovine serum (ATCC, 50-189-025NP) + 1× penicillin-streptomycin-glutamine (Gibco, 10378016) + 1× B27 supplement (Gibco, 17504044)] and counted using a hemocytometer and plated at appropriate densities onto chambers or wells that were incubated with laminin

(Sigma-Aldrich, L2020). CGNPs were cultured at 37°C, 5% $CO_2$, and 95% humidity in neuronal media. For activation of HH signaling, either SHH CM collected from COS-7 cells was added to the media (1:10) or 500 nM SAG (Enzo Life Sciences, ALX-270-426-M001) dissolved in dimethyl sulfoxide (DMSO) was added to the media. To antagonize HH signaling, BMP2 (PeproTech, 120-02) was used at 100 ng/ml, and BMP10 (PeproTech, 120-40) was used at 10 ng/ml. Half media changes were done every 24 hours for the duration of the cultures. Twenty-four hours before fixation, 10 μM EdU (Invitrogen, A10044), dissolved in DMSO, was administered to the culture.

### Genotyping with β-GAL fluorescence

For coculturing *Kif17*$^{+/-}$ and *Kif17*$^{-/-}$ CGNPs, we used BetaFluor β-gal assay kit (Promega, 70979-3) to distinguish between *Kif17*$^{+/-}$ and *Kif17*$^{-/-}$ littermates at P8. Briefly, while dissected cerebella were on ice in Hibernate-A media, half of the cortex were placed in TrypLE express (Invitrogen, ILT12604013) for 15 min at 37°C before lysing with reporter lysis buffer (Promega, E397A). Samples were spun at 15,000 rpm for 10 min at 4°C, and the supernatant was removed to a fresh tube. Lysates were then plated in triplicate in clear bottom 96-well plate and incubated with assay mixture for 30 min at 37°C before reading fluorescence. Genotyping samples taken at dissection later confirmed β-GAL assay results.

### CGNP culture immunofluorescence

Culture medium was removed gently before coverslips were fixed in 4% paraformaldehyde for 30 min at room temperature. Coverslips were washed three times for 5 min with 1X PBST$^X$ and then were stained with EdU staining solution [100 mM tris-HCl (pH 8.3), 0.5 mM $CuSO_4$, 50 mM ascorbic acid, 50 μM Alexa Fluor 555 azide, and triethylammonium salt (Thermo Fisher Scientific, A20012)] for 30 min at room temperature. Coverslips were washed three times for 5 min with 1X PBST$^X$ and then blocked with blocking buffer (3% bovine serum albumin, 1% heat-inactivated sheep serum, and 0.1% Triton X-100) for either 1 hour at room temperature or 4°C overnight. Primary antibodies were diluted in blocking buffer. Coverslips were removed from the plate and were placed onto the diluted primary antibodies on top of parafilm for 1 hour at room temperature. Coverslips were placed back in the well and were washed three times for 5 min with 1X PBST$^X$. Secondary antibodies were diluted in blocking buffer and were added to a fresh piece of parafilm. Coverslips were placed onto the parafilm and incubated with the secondaries for 1 hour at room temperature. After secondary incubation, nuclei were labeled using DAPI (0.5 ng/ml in block buffer) for 10 min. Coverslips were then washed three times for 5 min with PBST$^X$. Before mounting onto a slide with Immu-Mount aqueous mounting medium (Thermo Fisher Scientific, 9990412), coverslips were briefly dipped in water. Images were taken on a Leica SP5X upright confocal (two photon).

### CGNP microplate assays

To quantify EdU incorporation in vitro, a Click-iT EdU proliferation assay (Thermo Fisher Scientific, C10499) was used in CGNPs in vitro. Twenty-four hours after plating, EdU was added to the culture (10 μM, dissolved in DMSO). Forty-eight hours after plating, the assay was completed according to the manufacturer's protocol. To measure BrdU incorporation, the colorimetric BrdU Cell Proliferation ELISA Kit (Abcam, ab126556) was used. Forty-eight hours after plating (2 days in vitro), BrdU was administered to the culture. Forty-eight hours after BrdU addition (4 days in vitro), the assay was completed according to the manufacturer's protocol. To quantify the number of viable CGNPs in vitro, a CellTiter-Glo Luminescent Cell Viability Assay (Promega, G7570) was used on cultures grown for 4 days in vitro. The assay was performed according to the manufacturer's protocol.

### Immunoprecipitation of tagged proteins

COS-7 cells were transiently transfected with the relevant DNA constructs using Lipofectamine 2000 (Invitrogen, 11668). Cell lysates (1 mg) were precleared with Protein-G agarose beads (Roche, catalog number 11719416001) for 1 hour at 4°C. MYC- or HA-tagged proteins were immunoprecipitated from precleared lysates using either anti-MYC or anti-HA antibodies for 2 hours at 4°C. Following immunoprecipitation, the lysates were incubated with Protein-G agarose beads for 1 hour at 4°C. The Protein-G agarose beads were subjected to five 8-min washes in Hepes lysis buffer and resuspended in 30 μl of 1X PBS and 6X Laemmli buffer. The samples were boiled for 10 min, and proteins were separated using SDS-PAGE and analyzed by Western blotting. Visualization and quantitation were identical to the above-described Western blot analysis.

### Image quantitation

To quantify intensity of SHH immunofluorescent signal, ImageJ software was used to measure the fluorescence integrated density of individual PC bodies, subtracting the background measured from the internal granule layer. Per mouse, at least five images from the posterior lobes and five images of the anterior lobes were measured. To quantify fluorescent *Gli1* fluorescence, ImageJ software was used to measure the integrated density fluorescent signal contained to either the EGL (CGNPs) or lower molecular layer to inner granule layer (IGL, BG, and CGNs). At least six images were analyzed per mouse; three images for each posterior and anterior lobes. For all image analyses, images were blinded.

### Quantitation and statistical analysis

All the data are mean ± SD. All statistical analyses were performed using GraphPad Prism (www.graphpad.com). Statistical significance was determined by using a two-tailed Student's *t* test. For all the experimental analyses, a minimum of three mice of each genotype were analyzed, each *n* represents a mouse. For in vitro experiments, a minimum of three biological replicates were analyzed, each *n* represents a biological replicate. All the statistical details (statistical test used, adjusted *P* value, statistical significance, and exact value of each *n*) for each experiment are specified in the figure legends.

## Supplementary Materials

**This PDF file includes:**

Figs. S1 to S11
Tables S1 and S2
References

## REFERENCES AND NOTES

1. N. Dahmane, A. Ruiz i Altaba, Sonic hedgehog regulates the growth and patterning of the cerebellum. *Development* **126**, 3089–3100 (1999).
2. R. J. Wechsler-Reya, M. P. Scott, Control of neuronal precursor proliferation in the cerebellum by Sonic Hedgehog. *Neuron* **22**, 103–114 (1999).
3. P. M. Lewis, A. Gritli-Linde, R. Smeyne, A. Kottmann, A. P. McMahon, Sonic hedgehog signaling is required for expansion of granule neuron precursors and patterning of the mouse cerebellum. *Dev. Biol.* **270**, 393–410 (2004).

4. J. D. Corrales, S. Blaess, E. M. Mahoney, A. L. Joyner, The level of sonic hedgehog signaling regulates the complexity of cerebellar foliation. *Development* **133**, 1811–1821 (2006).
5. L. Izzi, M. Lévesque, S. Morin, D. Laniel, B. C. Wilkes, F. Mille, R. S. Krauss, A. P. McMahon, B. L. Allen, F. Charron, Boc and Gas1 each form distinct Shh receptor complexes with Ptch1 and are required for Shh-mediated cell proliferation. *Dev. Cell* **20**, 788–801 (2011).
6. J. D. Corrales, G. L. Rocco, S. Blaess, Q. Guo, A. L. Joyner, Spatial pattern of sonic hedgehog signaling through Gli genes during cerebellum development. *Development* **131**, 5581–5590 (2004).
7. F. Y. Cheng, J. T. Fleming, C. Chiang, Bergmann glial Sonic hedgehog signaling activity is required for proper cerebellar cortical expansion and architecture. *Dev. Biol.* **440**, 152–166 (2018).
8. F. Bangs, K. V. Anderson, Primary cilia and mammalian hedgehog signaling. *Cold Spring Harb. Perspect. Biol.* **9**, a028175 (2017).
9. S. Nonaka, Y. Tanaka, Y. Okada, S. Takeda, A. Harada, Y. Kanai, M. Kido, N. Hirokawa, Randomization of left-right asymmetry due to loss of nodal cilia generating leftward flow of extraembryonic fluid in mice lacking KIF3B motor protein. *Cell* **95**, 829–837 (1998).
10. S. Takeda, Y. Yonekawa, Y. Tanaka, Y. Okada, S. Nonaka, N. Hirokawa, Left-right asymmetry and kinesin superfamily protein KIF3A: New insights in determination of laterality and mesoderm induction by kif3A$^{-/-}$ mice analysis. *J. Cell Biol.* **145**, 825–836 (1999).
11. D. Huangfu, A. Liu, A. S. Rakeman, N. S. Murcia, L. Niswander, K. V. Anderson, Hedgehog signalling in the mouse requires intraflagellar transport proteins. *Nature* **426**, 83–87 (2003).
12. N. Spassky, Y. G. Han, A. Aguilar, L. Strehl, L. Besse, C. Laclef, M. Romaguera Ros, J. M. Garcia-Verdugo, A. Alvarez-Buylla, Primary cilia are required for cerebellar development and Shh-dependent expansion of progenitor pool. *Dev. Biol.* **317**, 246–259 (2008).
13. B. S. Carpenter, R. L. Barry, K. J. Verhey, B. L. Allen, The heterotrimeric kinesin-2 complex interacts with and regulates GLI protein function. *J. Cell Sci.* **128**, 1034–1050 (2015).
14. N. Hirokawa, Y. Noda, Y. Tanaka, S. Niwa, Kinesin superfamily motor proteins and intracellular transport. *Nat. Rev. Mol. Cell Biol.* **10**, 682–696 (2009).
15. M. He, S. Agbu, K. V. Anderson, Microtubule motors drive hedgehog signaling in primary cilia. *Trends Cell Biol.* **27**, 110–125 (2017).
16. Z. Yang, E. A. Roberts, L. S. Goldstein, Functional analysis of mouse kinesin motor Kif3C. *Mol. Cell. Biol.* **21**, 5306–5311 (2001).
17. X. Yin, Y. Takei, M. A. Kido, N. Hirokawa, Molecular motor KIF17 is fundamental for memory and learning via differential support of synaptic NR2A/2B levels. *Neuron* **70**, 310–325 (2011).
18. M. F. Engelke, B. Waas, S. E. Kearns, A. Suber, A. Boss, B. L. Allen, K. J. Verhey, Acute inhibition of heterotrimeric kinesin-2 function reveals mechanisms of intraflagellar transport in mammalian cilia. *Curr. Biol.* **29**, 1137–1148.e4 (2019).
19. D. Signor, K. P. Wedaman, L. S. Rose, J. M. Scholey, Two heteromeric kinesin complexes in chemosensory neurons and sensory cilia of Caenorhabditis elegans. *Mol. Biol. Cell* **10**, 345–360 (1999).
20. J. J. Snow, G. Ou, A. L. Gunnarson, M. R. S. Walker, H. M. Zhou, I. Brust-Mascher, J. M. Scholey, Two anterograde intraflagellar transport motors cooperate to build sensory cilia on C. elegans neurons. *Nat. Cell Biol.* **6**, 1109–1113 (2004).
21. C. Insinna, N. Pathak, B. Perkins, I. Drummond, J. C. Besharse, The homodimeric kinesin, Kif17, is essential for vertebrate photoreceptor sensory outer segment development. *Dev. Biol.* **316**, 160–170 (2008).
22. T. R. Lewis, S. R. Kundinger, A. L. Pavlovich, J. R. Bostrom, B. A. Link, J. C. Besharse, Cos2/Kif7 and Osm-3/Kif17 regulate onset of outer segment development in zebrafish photoreceptors through distinct mechanisms. *Dev. Biol.* **425**, 176–190 (2017).
23. T. R. Lewis, S. R. Kundinger, B. A. Link, C. Insinna, J. C. Besharse, Kif17 phosphorylation regulates photoreceptor outer segment turnover. *BMC Cell Biol.* **19**, 25 (2018).
24. C. Zhao, Y. Omori, K. Brodowska, P. Kovach, J. Malicki, Kinesin-2 family in vertebrate ciliogenesis. *Proc. Natl. Acad. Sci. U.S.A.* **109**, 2388–2393 (2012).
25. X. Yin, X. Feng, Y. Takei, N. Hirokawa, Regulation of NMDA receptor transport: A KIF17-cargo binding/releasing underlies synaptic plasticity and memory in vivo. *J. Neurosci.* **32**, 5486–5499 (2012).
26. B. D. Harfe, P. J. Scherz, S. Nissim, H. Tian, A. P. McMahon, C. J. Tabin, Evidence for an expansion-based temporal Shh gradient in specifying vertebrate digit identities. *Cell* **118**, 517–528 (2004).
27. E. Bowie, S. C. Goetz, TTBK2 and primary cilia are essential for the connectivity and survival of cerebellar Purkinje neurons. *eLife* **9**, e51166 (2020).
28. E. T. Hall, M. E. Dillard, D. P. Stewart, Y. Zhang, B. Wagner, R. M. Levine, S. M. Pruett-Miller, A. Sykes, J. Temirov, R. E. Cheney, M. Mori, C. G. Robinson, S. K. Ogden, Cytoneme delivery of Sonic Hedgehog from ligand-producing cells requires Myosin 10 and a Dispatched-BOC/CDON co-receptor complex. *eLife* **10**, e61432 (2021).
29. A. Kawakami, Y. Nojima, A. Toyoda, M. Takahoko, M. Satoh, H. Tanaka, H. Wada, I. Masai, H. Terasaki, Y. Sakaki, H. Takeda, H. Okamoto, The zebrafish-secreted matrix protein you/scube2 is implicated in long-range regulation of hedgehog signaling. *Curr. Biol.* **15**, 480–488 (2005).
30. G. E. Hollway, J. Maule, P. Gautier, T. M. Evans, D. G. Keenan, C. Lohs, D. Fischer, C. Wicking, P. D. Currie, Scube2 mediates Hedgehog signalling in the zebrafish embryo. *Dev. Biol.* **294**, 104–118 (2006).
31. H. Y. Lee, L. A. Greene, C. A. Mason, M. C. Manzini, Isolation and culture of post-natal mouse cerebellar granule neuron progenitor cells and neurons. *J. Vis. Exp.*, 990 (2009).
32. D. Huangfu, K. V. Anderson, Cilia and Hedgehog responsiveness in the mouse. *Proc. Natl. Acad. Sci. U.S.A.* **102**, 11325–11330 (2005).
33. V. Matei, S. Pauley, S. Kaing, D. Rowitch, K. W. Beisel, K. Morris, F. Feng, K. Jones, J. Lee, B. Fritzsch, Smaller inner ear sensory epithelia in Neurog 1 null mice are related to earlier hair cell cycle exit. *Dev. Dyn.* **234**, 633–650 (2005).
34. T. Jiwani, J. J. Kim, N. D. Rosenblum, Suppressor of fused controls cerebellum granule cell proliferation by suppressing Fgf8 and spatially regulating Gli proteins. *Development* **147**, dev170274 (2020).
35. H. Tukachinsky, L. V. Lopez, A. Salic, A mechanism for vertebrate Hedgehog signaling: Recruitment to cilia and dissociation of SuFu-Gli protein complexes. *J. Cell Biol.* **191**, 415–428 (2010).
36. J. Svard, K. Heby-Henricson, M. Persson-Lek, B. Rozell, M. Lauth, A. Bergström, J. Ericson, R. Toftgård, S. Teglund, Genetic elimination of Suppressor of fused reveals an essential repressor function in the mammalian Hedgehog signaling pathway. *Dev. Cell* **10**, 187–197 (2006).
37. C. H. Chang, M. Zanini, H. Shirvani, J. S. Cheng, H. Yu, C. H. Feng, A. L. Mercier, S. Y. Hung, A. Forget, C. H. Wang, S. M. Cigna, I. L. Lu, W. Y. Chen, S. Leboucher, W. J. Wang, M. Ruat, N. Spassky, J. W. Tsai, O. Ayrault, Atoh1 controls primary cilia formation to allow for SHH-triggered granule neuron progenitor proliferation. *Dev. Cell* **48**, 184–199.e5 (2019).
38. C. Cruz, V. Ribes, E. Kutejova, J. Cayuso, V. Lawson, D. Norris, J. Stevens, M. Davey, K. Blight, F. Bangs, A. Mynett, E. Hirst, R. Chung, N. Balaskas, S. L. Brody, E. Marti, J. Briscoe, Foxj1 regulates floor plate cilia architecture and modifies the response of cells to sonic hedgehog signalling. *Development* **137**, 4271–4282 (2010).
39. K. A. Peterson, Y. Nishi, W. Ma, A. Vedenko, L. Shokri, X. Zhang, M. McFarlane, J. M. Baizabal, J. P. Junker, A. van Oudenaarden, T. Mikkelsen, B. E. Bernstein, T. L. Bailey, M. L. Bulyk, W. H. Wong, A. P. McMahon, Neural-specific Sox2 input and differential Gli-binding affinity provide context and positional information in Shh-directed neural patterning. *Genes Dev.* **26**, 2802–2816 (2012).
40. I. Rios, R. Alvarez-Rodriguez, E. Marti, S. Pons, Bmp2 antagonizes sonic hedgehog-mediated proliferation of cerebellar granule neurones through Smad5 signalling. *Development* **131**, 3159–3168 (2004).
41. C. Ogawa, S. Mikawa, S. Li, Y. Hayashi, K. Masumoto, K. Sato, BMP10 expression in the adult rat central nervous system. *J. Chem. Neuroanat.* **121**, 102084 (2022).
42. J. J. Lee, S. C. Ekker, D. P. von Kessler, J. A. Porter, B. I. Sun, P. A. Beachy, Autoproteolysis in hedgehog protein biogenesis. *Science* **266**, 1528–1537 (1994).
43. D. A. Bumcrot, R. Takada, A. P. McMahon, Proteolytic processing yields two secreted forms of sonic hedgehog. *Mol. Cell. Biol.* **15**, 2294–2303 (1995).
44. J. A. Porter, D. P. von Kessler, S. C. Ekker, K. E. Young, J. J. Lee, K. Moses, P. A. Beachy, The product of hedgehog autoproteolytic cleavage active in local and long-range signalling. *Nature* **374**, 363–366 (1995).
45. K. Petrov, B. M. Wierbowski, A. Salic, Sending and receiving hedgehog signals. *Annu. Rev. Cell Dev. Biol.* **33**, 145–168 (2017).
46. T. Chu, M. Chiu, E. Zhang, S. Kunes, A C-terminal motif targets Hedgehog to axons, coordinating assembly of the Drosophila eye and brain. *Dev. Cell* **10**, 635–646 (2006).
47. S. Blaess, D. Stephen, A. L. Joyner, Gli3 coordinates three-dimensional patterning and growth of the tectum and cerebellum by integrating Shh and Fgf8 signaling. *Development* **135**, 2093–2103 (2008).
48. S. Endoh-Yamagami, M. Evangelista, D. Wilson, X. Wen, J. W. Theunissen, K. Phamluong, M. Davis, S. J. Scales, M. J. Solloway, F. J. de Sauvage, A. S. Peterson, The mammalian Cos2 homolog Kif7 plays an essential role in modulating Hh signal transduction during development. *Curr. Biol.* **19**, 1320–1326 (2009).
49. J. F. Dishinger, H. L. Kee, P. M. Jenkins, S. Fan, T. W. Hurd, J. W. Hammond, Y. N. T. Truong, B. Margolis, J. R. Martens, K. J. Verhey, Ciliary entry of the kinesin-2 motor KIF17 is regulated by importin-beta2 and RanGTP. *Nat. Cell Biol.* **12**, 703–710 (2010).
50. X. Wen, C. K. Lai, M. Evangelista, J. A. Hongo, F. J. de Sauvage, S. J. Scales, Kinetics of hedgehog-dependent full-length Gli3 accumulation in primary cilia and subsequent degradation. *Mol. Cell. Biol.* **30**, 1910–1922 (2010).
51. N. Santos, J. F. Reiter, A central region of Gli2 regulates its localization to the primary cilium and transcriptional activity. *J. Cell Sci.* **127**, 1500–1510 (2014).
52. F. Haque, C. Freniere, Q. Ye, N. Mani, E. M. Wilson-Kubalek, P. I. Ku, R. A. Milligan, R. Subramanian, Cytoskeletal regulation of a transcription factor by DNA mimicry via coiled-coil interactions. *Nat. Cell Biol.* **24**, 1088–1098 (2022).
53. Q. Ding, S. I. Fukami, X. Meng, Y. Nishizaki, X. Zhang, H. Sasaki, A. Dlugosz, M. Nakafuku, C. C. Hui, Mouse suppressor of fused is a negative regulator of sonic hedgehog signaling and alters the subcellular distribution of Gli1. *Curr. Biol.* **9**, 1119–1122 (1999).
54. M. Tuson, M. He, K. V. Anderson, Protein kinase A acts at the basal body of the primary cilium to prevent Gli2 activation and ventralization of the mouse neural tube. *Development* **138**, 4921–4930 (2011).

55. M. He, R. Subramanian, F. Bangs, T. Omelchenko, K. F. Liem Jr., T. M. Kapoor, K. V. Anderson, The kinesin-4 protein Kif7 regulates mammalian Hedgehog signalling by organizing the cilium tip compartment. *Nat. Cell Biol.* **16**, 663–672 (2014).
56. S. Wang, Y. Tanaka, Y. Xu, S. Takeda, N. Hirokawa, KIF3B promotes a PI3K signaling gradient causing changes in a Shh protein gradient and suppressing polydactyly in mice. *Dev. Cell* **57**, 2273–2289.e11 (2022).
57. R. Machold, S. Hayashi, M. Rutlin, M. D. Muzumdar, S. Nery, J. G. Corbin, A. Gritli-Linde, T. Dellovade, J. A. Porter, L. L. Rubin, H. Dudek, A. P. McMahon, G. Fishell, Sonic hedgehog is required for progenitor cell maintenance in telencephalic stem cell niches. *Neuron* **39**, 937–950 (2003).
58. J. J. Breunig, M. R. Sarkisian, J. I. Arellano, Y. M. Morozov, A. E. Ayoub, S. Sojitra, B. Wang, R. A. Flavell, P. Rakic, T. Town, Primary cilia regulate hippocampal neurogenesis by mediating sonic hedgehog signaling. *Proc. Natl. Acad. Sci. U.S.A.* **105**, 13127–13132 (2008).
59. Y. G. Han, N. Spassky, M. Romaguera-Ros, J. M. Garcia-Verdugo, A. Aguilar, S. Schneider-Maunoury, A. Alvarez-Buylla, Hedgehog signaling and primary cilia are required for the formation of adult neural stem cells. *Nat. Neurosci.* **11**, 277–284 (2008).
60. S. Ahn, A. L. Joyner, In vivo analysis of quiescent adult neural stem cells responding to Sonic hedgehog. *Nature* **437**, 894–897 (2005).
61. B. Macho, S. Brancorsini, G. M. Fimia, M. Setou, N. Hirokawa, P. Sassone-Corsi, CREM-dependent transcription in male germ cells controlled by a kinesin. *Science* **298**, 2388–2390 (2002).
62. V. Chennathukuzhi, C. R. Morales, M. El-Alfy, N. B. Hecht, The kinesin KIF17b and RNA-binding protein TB-RBP transport specific cAMP-responsive element modulator-regulated mRNAs in male germ cells. *Proc. Natl. Acad. Sci. U.S.A.* **100**, 15566–15571 (2003).
63. S. Kimmins, N. Kotaja, G. Fienga, U. S. Kolthur, S. Brancorsini, K. Hogeveen, L. Monaco, P. Sassone-Corsi, A specific programme of gene transcription in male germ cells. *Reprod. Biomed. Online* **8**, 496–500 (2004).
64. N. Kotaja, H. Lin, M. Parvinen, P. Sassone-Corsi, Interplay of PIWI/Argonaute protein MIWI and kinesin KIF17b in chromatoid bodies of male germ cells. *J. Cell Sci.* **119**, 2819–2825 (2006).
65. M. Saade, M. Irla, J. Govin, G. Victorero, M. Samson, C. Nguyen, Dynamic distribution of Spatial during mouse spermatogenesis and its interaction with the kinesin KIF17b. *Exp. Cell Res.* **313**, 614–626 (2007).
66. A. M. Clark, K. K. Garland, L. D. Russell, Desert hedgehog (Dhh) gene is required in the mouse testis for formation of adult-type Leydig cells and normal development of peritubular cells and seminiferous tubules. *Biol. Reprod.* **63**, 1825–1838 (2000).
67. Y. Wu, C. Wang, H. Sun, D. LeRoith, S. Yakar, High-efficient FLPo deleter mice in C57BL/6J background. *PLOS ONE* **4**, e8054 (2009).
68. B. L. Allen, J. Y. Song, L. Izzi, I. W. Althaus, J. S. Kang, F. Charron, R. S. Krauss, A. P. McMahon, Overlapping roles and collective requirement for the coreceptors GAS1, CDO, and BOC in SHH pathway function. *Dev. Cell* **20**, 775–787 (2011).
69. D. G. Wilkinson, In situ hybridization: a practical approach. (*Oxford; New York: IRL Press at Oxford University Press, 1992*) .
70. S. Trifonov, Y. Yamashita, M. Kase, M. Maruyama, T. Sugimoto, Overview and assessment of the histochemical methods and reagents for the detection of β-galactosidase activity in transgenic animals. *Anat. Sci. Int.* **91**, 56–67 (2016).
71. B. B. Madison, K. Braunstein, E. Kuizon, K. Portman, X. T. Qiao, D. L. Gumucio, Epithelial hedgehog signals pattern the intestinal crypt-villus axis. *Development* **132**, 279–289 (2005).
72. T. Shimokawa, U. Tostar, M. Lauth, R. Palaniswamy, M. Kasper, R. Toftgård, P. G. Zaphiropoulos, Novel human glioma-associated oncogene 1 (GLI1) splice variants reveal distinct mechanisms in the terminal transduction of the hedgehog signal. *J. Biol. Chem.* **283**, 14345–14354 (2008).
73. F. Mille, L. Tamayo-Orrego, M. Lévesque, M. Remke, A. Korshunov, J. Cardin, N. Bouchard, L. Izzi, M. Kool, P. A. Northcott, M. D. Taylor, S. M. Pfister, F. Charron, The Shh receptor Boc promotes progression of early medulloblastoma to advanced tumors. *Dev. Cell* **31**, 34–47 (2014).
74. Y.-C. Lin, S. R. Roffler, Y.-T. Yan, R.-B. Yang, Disruption of *Scube2* impairs endochondral bone formation. *J. Bone Miner. Res.* **30**, 1255–1267 (2015).
75. Y. Liu, S. Y. du, M. Ding, X. Dou, F. F. Zhang, Z. Y. Wu, S. W. Qian, W. Zhang, Q. Q. Tang, C. J. Xu, The BMP4-Smad signaling pathway regulates hyperandrogenism development in a female mouse model. *J. Biol. Chem.* **292**, 11740–11750 (2017).
76. C. H. H. Hor, J. C. W. Lo, A. L. S. Cham, W. Y. Leong, E. L. K. Goh, Multifaceted functions of Rab23 on primary cilium-mediated and hedgehog signaling-mediated cerebellar granule cell proliferation. *J. Neurosci.* **41**, 6850–6863 (2021).
77. M. K. Scales, A. Velez-Delgado, N. G. Steele, H. E. Schrader, A. M. Stabnick, W. Yan, N. M. Mercado Soto, Z. C. Nwosu, C. Johnson, Y. Zhang, D. J. Salas-Escabillas, R. E. Menjivar, H. C. Maurer, H. C. Crawford, F. Bednar, K. P. Olive, M. Pasca di Magliano, B. L. Allen, Combinatorial Gli activity directs immune infiltration and tumor growth in pancreatic cancer. *PLOS Genet.* **18**, e1010315 (2022).
78. Y. Han, Y. Xiong, X. Shi, J. Wu, Y. Zhao, J. Jiang, Regulation of Gli ciliary localization and Hedgehog signaling by the PY-NLS/karyopherin-β2 nuclear import system. *PLOS Biol.* **15**, e2002063 (2017).


**Acknowledgments:** We thank past and present Allen laboratory members for the valuable feedback and suggestions. We also thank J. Besharse (Medical College of Wisconsin) for providing the *Kif17* mutant mice. We thank A. Salic (Harvard) for sharing the SUFU antibody. We thank S. Scales (Genentech) and M. Engelke (Illinois State University) for the insightful comments. We thank R. Passino (University of Michigan) for technical assistance with the CGNP assays. We thank members of the Department of Cell and Developmental Biology who provided access to equipment, including the O'Shea, Engel, and Spence laboratories. PAX6 and LIM1/2 antibodies were obtained from the Developmental Studies Hybridoma Bank, created by the Eunice Kennedy Shriver National Institute of Child Health and Human Development of the National Institutes of Health and maintained at The University of Iowa, Department of Biology, Iowa City, IA 52242, USA. Last, we acknowledge the Biomedical Research Core Facilities Microscopy Core, which is supported by the Rogel Cancer Center, for providing access to confocal microscopy equipment. **Funding:** This work was supported by the National Institutes of Health grant R01GM118751 (to B.L.A. and K.J.V.), National Institutes of Health training program grants T32GM008353 (to B.W.) and T32HD007505 (to B.W.), and Bradley Merrill Patten Memorial Scholarship (to B.W.). **Author contributions:** Conceptualization: B.W. and B.L.A. Data curation: B.W., B.S.C., and N.E.F. Formal analysis: B.W. and N.E.F. Funding acquisition: B.W. and B.L.A. Investigation: B.W., B.S.C., and B.L.A. Methodology: B.W. Project administration: B.L.A. Resources: K.J.V. Supervision: B.L.A. Validation: B.W. Visualization: O.Q.M. Writing/editing: B.W. and B.L.A. **Competing interests:** The authors declare that they have no competing interests. **Data and materials availability:** All data needed to evaluate the conclusions in the paper are present in the paper and/or the Supplementary Materials.

Submitted 29 July 2022
Accepted 26 March 2024
Published 26 April 2024
10.1126/sciadv.ade1650